



**HAL**  
open science

# Efficient Configuration of Heterogeneous Multistatic Sonar Networks: a Mixed-Integer Linear Programming Approach

Owein Thuillier, Nicolas Le Josse, Alexandru-Liviu Olteanu, Marc Sevaux,  
Hervé Tanguy

► **To cite this version:**

Owein Thuillier, Nicolas Le Josse, Alexandru-Liviu Olteanu, Marc Sevaux, Hervé Tanguy. Efficient Configuration of Heterogeneous Multistatic Sonar Networks: a Mixed-Integer Linear Programming Approach. *Computers and Operations Research*, 2024, 167, pp.106637. 10.1016/j.cor.2024.106637 . hal-04538278

**HAL Id: hal-04538278**

**<https://hal.science/hal-04538278v1>**

Submitted on 9 Apr 2024

**HAL** is a multi-disciplinary open access archive for the deposit and dissemination of scientific research documents, whether they are published or not. The documents may come from teaching and research institutions in France or abroad, or from public or private research centers.

L'archive ouverte pluridisciplinaire **HAL**, est destinée au dépôt et à la diffusion de documents scientifiques de niveau recherche, publiés ou non, émanant des établissements d'enseignement et de recherche français ou étrangers, des laboratoires publics ou privés.

# Efficient Configuration of Heterogeneous Multistatic Sonar Networks: a Mixed-Integer Linear Programming Approach

Owein THUILLIER<sup>a,b,\*</sup>, Nicolas LE JOSSE<sup>a</sup>, Alexandru-Liviu OLTEANU<sup>b</sup>, Marc SEVAUX<sup>b</sup>, Hervé TANGUY<sup>a</sup>

<sup>a</sup> *Thales, Defence and Mission Systems, Brest, France*

*{owein.thuillier, nicolas.lejosse, herve.tanguy}@fr.thalesgroup.com*

<sup>b</sup> *Université Bretagne-Sud, Lab-STICC, UMR CNRS 6285, Lorient, France*

*{owein.thuillier, alexandru.olteanu, marc.sevaux}@univ-ubs.fr*

---

## Abstract

The work undertaken in this paper pertains to the optimal spatial configuration of a heterogeneous Wireless Sensor Network (WSN) for the Area Coverage (AC) problem. Specifically, this research falls under the heading of Anti-Submarine Warfare (ASW) with an emphasis on active sonar systems and, more pointedly still, on a specific type of sensor: sonobuoys (portmanteau word formed by “sonar” and “buoy”). These buoys are further divided into three main categories: transmitter-only (Tx), receiver-only (Rx) and transmitter-receiver (TxRx). In this paper, we will therefore try to determine the geographical location of the different buoys comprising a Multistatic Sonar Network (MSN), special case of WSN, so as to maximize the overall surface area covered. To do this, we discretize an Area of Interest (AoI) into regular cells using bathymetric and altimetric data, and place a deployment position and a fictitious target at the center of each cell so that we can evaluate the network’s performance. More precisely, we are taking into account a limited number of sensors (buoys) with possible pairwise incompatibilities, variable performances, probabilistic detection models, an adverse masking effect (direct blast) as well as coastlines features. Finally, in order to solve this problem, we have developed several efficient Mixed-Integer Linear Programs (MILPs), all of which have been thoroughly tried-and-tested on a benchmark set of 100 instances derived from real elevation data. This has led us to identify an ideal model, i.e. one that is significantly better than all the others in the statistical sense.

*Keywords:* OR in defense, multistatic sonar networks, heterogeneous sensors, area coverage problem, mixed-integer linear programming

---

---

\*Corresponding author.

*Email address:* [owein.thuillier@fr.thalesgroup.com](mailto:owein.thuillier@fr.thalesgroup.com) (Owein THUILLIER)

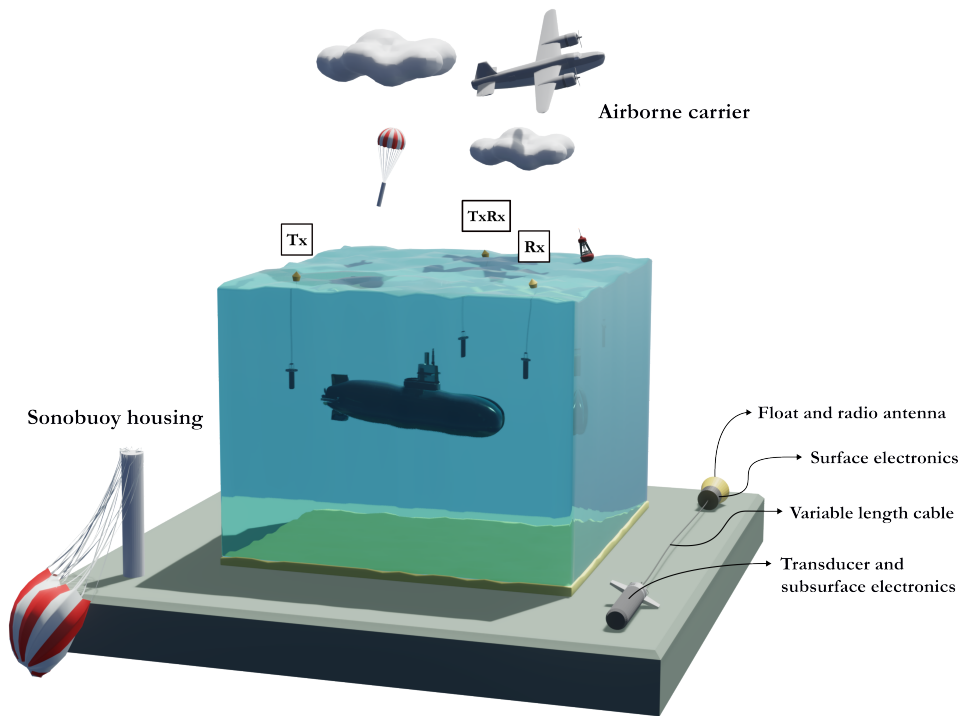


Figure 1: Streamlined illustration of the overall operating environment.

## 1. Introduction

In airborne Anti-Submarine Warfare (ASW), the challenge of finding optimal deployment patterns for networked sonars is of particular importance when it comes to conducting effective search operations against underwater threats or even for carrying out wide-area surveillance [4, 47, 54, 55, 58].

More precisely, this work focus on this subject while laying special emphasis upon active sonar systems, i.e. with emission of a sound pulse and reception of the reflected wave on the target, commonly referred to as echo (see [11, 44, 59] for a comprehensive introduction to underwater acoustics). For such active systems, there exist two separate geometrical configurations depending on the spatial arrangement of the source–receiver pair. The configuration is said to be monostatic when the two components are collocated (i.e. a single full-fledged sensor) and bistatic when they are non-collocated, i.e. two separate sensors located at two distinct geographical sites, sometimes several kilometres apart and possibly at different operating depths [11, 59]. A special case of bistatism exists when the angle subtended by the source–receiver segment from the target perspective (i.e. bistatic angle) is close to 0: this is referred to as quasi-monostatism or pseudo-monostatism

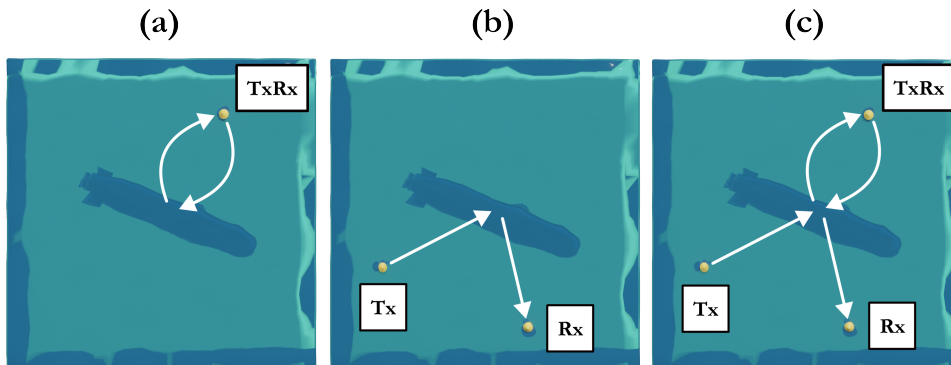


Figure 2: Monostatic (a), bistatic (b) and multistatic (c) configurations.

in the literature [31].

Furthermore, in this work, we will confine ourselves to the case study of a specific type of sonar, also known as underwater ears [33]: the sonobuoys (portmanteau word formed by “sonar” and “buoy”). The latter are cylinder-shaped, consumable acoustic sensors dropped from an airborne carrier such as a Maritime Patrol Aircraft (MPA), a helicopter or even an Unmanned Aerial Vehicle (UAV). Upon impact with the sea surface, a deployment sequence is then initiated and within which the acoustic heads are lowered to a predetermined depth from a discrete range of options, which can be further adjusted through remote control activations depending on the buoy model [33]. Indeed, by means of a floating unit housing the UHF/VHF radio antenna [33], the airborne carrier is able to interact with them throughout the area, albeit within a limited communication range (buoy-dependent). A simplified illustration of the operational context is available in Figure 1. In addition, these aforementioned buoys are further divided into the following three broad categories: transmitter-only<sup>1</sup> (Tx), receiver-only (Rx) and transmitter-receiver (TxRx), sometimes referred to as post in the related literature [12, 21, 51]. Within each of these categories, there is a variety of different types of buoys [33, 34, 36], all with their own intrinsic characteristics (e.g. emission frequency, lifetime, emission power, immersion depth etc.), which underpins the idea of addressing the heterogeneous sensor scenario.

Indeed, in ASW surveillance missions, an MPA would logically try to use homogeneous sensors to simplify pattern conception and buoys deployment. Yet, heterogeneous sensors are of interest for different reasons. MPA

<sup>1</sup>Note that the terms source and transmitter can be used interchangeably.



missions variety imply that various types of sonobuoys would be embarked: active or passive buoys with various characteristics in terms of bandwidth, directivity and sensitivity. A mission may change from the initial assignment without possibility to resupply, hence the need to exploit the available buoys onboard and to manage possibly incompatible buoys and heterogeneous sensors. Furthermore, sonar performance vary with environmental conditions, especially bottom depth: an Area of Interest (AoI) may be composed of a low depth region and a higher depth region, leading to different active sonar frequencies in those regions.

With these assumptions, we can henceforward define formally a MSN as a collection of active sonar systems in monostatic and/or bistatic configuration, the latter being a generalization of the former [11, 38, 55, 60, 61]. In the present case study, such sonar systems arise from the pairing of a source and a receiver stemming from one and the same buoy (Figure 2.a) or from two separate ones (Figure 2.b). Indeed, a sonar system in bistatic configuration might, for example, be comprised of the source of a Tx buoy and the receiver of a TxRx buoy, assuming pairwise compatibility<sup>2</sup>. Figure 2 shows an illustration of monostatic (a), bistatic (b) and multistatic (c) configurations respectively.

In this paper, we will therefore address the Area Coverage (AC) problem that is frequently encountered in the literature related to MSNs and, to a greater extent, in Wireless Sensor Networks (WSNs) [17, 41, 53]. Barrier Coverage (BC) and Point Coverage (PC) problems are also found in the WSN literature. The primary aim of AC involves ensuring a uniformly high level of monitoring over a designated AoI. In contrast, BC focuses on optimizing coverage along specific line segments or belt-shaped areas to prevent intrusions. Meanwhile, PC, also known as target coverage, aims at achieving maximum or specified coverage levels for particular points of interest, which could be potential targets or vital installations. A literature review on these three problems in the case of MSNs has been carried out in [57]. Here, we deal with the scenario of heterogeneous sensors, in limited number, alongside with probabilistic detection models and with the inclusion of certain adverse effects proper to underwater acoustic such as the direct blast effect [11]. The case of heterogeneous sensors is not inherent to MSNs, it is also ubiquitous in the literature related to WSNs as discussed in [30]. In addition, we will also take into account coastline features as well as particularities inherent to the heterogeneity of the sensors at hand, such as variable performance between source–receiver pairs and potential pairwise inter-incompatibilities

---

<sup>2</sup>From a practical point of view, incompatibilities may occur, for example between two sonars operating at different frequencies.

(e.g. between a high-frequency sensor and a low-frequency sensor). The overall objective is to maximize the total surface area covered by the MSN thus established.

To solve this problem, we will first discretize a given AoI with a certain granularity through bathymetric and topographic data, giving us a Digital Elevation Model (DEM), or, in more straightforward terms: a regular rectangular grid [29]. Then, we will reduce the AC problem to a PC problem by assigning a fictitious/dummy target and a deployment position to the center of each grid cell (see Section 2 for a formal description), as it was originally done in [14] or in [25]. In this way, it will be possible to assess the performance of the network across a range of appropriately distributed points. Hence, the finer the discretization, the more accurate the placement.

In the literature and to the best of our knowledge, the problem of placing heterogeneous sensors in the context of MSNs has never been addressed. It is therefore the first time it is formalized and solved. This enables variable performances to be taken into account, depending on the source–receiver pair under consideration, as well as possible incompatibilities. See [12–14, 25, 57] for the most recent literature dealing with coverage issues in MSNs. Similarly, the problem of placing sonars that can explicitly be buoys of three different categories (Tx, Rx, TxRx) has never been addressed either. Indeed, a simplification is regularly adopted and consists in considering only sources and receivers directly, i.e. Tx and Rx buoys. Furthermore, we also take into account some rarely considered aspects such as the direct blast effect, coastlines features and probabilistic detection models, whether taken independently or in combination. It should be noted that the drift of the buoys due to ocean currents is neglected and that the environment is 2D and homogeneous (identical environmental conditions at all points), as in the above-mentioned literature in the context of MSN configuration. More specifically, this work is a direct sequel to [25] and [57], which both dealt with the case of homogeneous sensors and did not distinguish between Tx, Rx and TxRx buoys per se. In terms of methods, we extend the linearizations of [50] used in [25]<sup>3</sup> to deal with the heterogeneous case plus the presence of TxRx buoys and thus propose a number of improved models (7) alongside with base (naïve) models (2). Following the analysis methodology adopted in [25], this has led us to identify an ideal model, i.e. one that is significantly better than all the others in the statistical sense.

Finally, this research is of operational interest, since effective algorithms

---

<sup>3</sup>Among the different linearizations studied in [25], the linearization based on [50] was indeed identified as the best performing for this problem.

for buoys pattern design may be useful in different phases of MPA missions: before-flight tactics design and planification, and on board redesign of patterns, when environmental conditions have been measured and do not correspond to expectation. It is with this in mind that we propose a set of methods and new considerations, hitherto unexplored.

The paper is organized as follows. In Section 2, we present several Mixed Integer Linear Programs (MILPs), introducing preliminary notations, some elements of multistatic detection theory and a core linearization. Then, in Section 3, we conduct a series of experiments in order to test the proposed formulations on a set of real instances. Finally, in Section 4, we conclude and give some perspectives for future research.

## 2. Compendium of Mathematical Formulations

### 2.1. Prerequisites

We begin by introducing some prerequisites, in particular concerning the notations employed, some theoretical elements of multistatic detection and a core linearization.

#### 2.1.1. Notations

Let  $m \in \mathbb{N}^*$  be the number of maritime cells in the regular rectangular grid (DEM) resulting from the discretization of a given AoI. We then have  $E = \{e_1, \dots, e_m\} \subseteq \mathbb{R}^2$  the set of possible deployment positions and  $T = \{t_1, \dots, t_m\} \subseteq \mathbb{R}^2$  the set of dummy targets, i.e. a target and a deployment position in the center of each maritime cell. As a reminder, these dummy targets enable network performance to be assessed at a set of regularly spaced points.

We then introduce the following notations for the three categories of buoys that may be found:

- $Tx$  the set of buoys types in the transmitter-only category,
- $Rx$  the set of buoys types in the receiver-only category and, finally,
- $TxRx$  the set of buoys types in the transmitter-receiver category.

Additionally, we have  $n_{Tx}^i \in \mathbb{N}^*$  the number of transmitter-only buoys of type  $i \in Tx$ ,  $n_{Rx}^i \in \mathbb{N}^*$  the number of receiver-only buoys of type  $i \in Rx$  and  $n_{TxRx}^i \in \mathbb{N}^*$  the number of transmitter-receiver buoys of type  $i \in TxRx$ .

Moreover, for practical reasons, in the following, we set  $I = Tx \cup TxRx$  and  $J = Rx \cup TxRx$  corresponding respectively to the set of buoys types with a source and the set of buoys types with a receiver. The reason behind

this choice is that a sonar system is formed by a source–receiver pair, regardless of their native buoys. Indeed, as stated earlier, a sonar system can be composed of the source of a TxRx buoy (or Tx) and the receiver of an Rx buoy (or TxRx).

Henceforth, we can introduce the set of admissible solutions (i.e. networks), which is formally defined as

$$\Omega = \{(S, R) \mid S \subseteq E \times I, R \subseteq E \times J, (2), (3), (7), (8), (9)\}, \quad (1)$$

where

$$\forall (e, i) \in E \times TxRx, (e, i) \in S \iff (e, i) \in R, \quad (2)$$

$$\forall e \in E, (4) + (5) + (6) \leq 1, \quad (3)$$

$$|\{(e, i) \in S \setminus R\}| \quad (4)$$

$$|\{(e, i) \in R \setminus S\}| \quad (5)$$

$$|\{(e, i) \in S \cap R\}| \quad (6)$$

$$\forall i \in Tx, |\{(e, i) \in S \setminus R\}| \leq n_{Tx}^i, \quad (7)$$

$$\forall i \in Rx, |\{(e, i) \in R \setminus S\}| \leq n_{Rx}^i, \quad (8)$$

$$\forall i \in TxRx, |\{(e, i) \in S \cap R\}| \leq n_{TxRx}^i. \quad (9)$$

In the above, S corresponds to buoys that can act as a source (TxRx or Tx) and R corresponds to buoys that can act as a receiver (TxRx or Rx). Then, (2) means that a source attached to a TxRx buoy can be deployed if and only if the associated receiver is also deployed (the two constituting one and the same buoy). In other words, a TxRx buoy must be present in both sets S and R. Equation (3) means that only one buoy may be deployed on a given deployment position where (4), (5) and (6) correspond respectively to the number of Tx, Rx and TxRx buoys. Indeed, the sets  $S \setminus R$ ,  $R \setminus S$  and  $S \cap R$  correspond respectively to the set of Tx, Rx and TxRx buoys deployed on the AoI. Finally, (7), (8) and (9) are capacity constraints on the number of buoys available for each of the three categories (Tx, Rx and TxRx).

Furthermore, we introduce the set of all possible sonar systems, which is explicitly defined as

$$\Xi = \{(s, r) \mid s = (e, i) \in E \times I, r = (e', j) \in E \times J, (i, j) \in C\}, \quad (10)$$

where  $C \subseteq I \times J$  is the set of functional sonar systems, in the sense

of compatibility (hardware or software) between source and receiver. Thus,  $(i, j) \in C$  means that it is possible to form a functional sonar system from a source of type  $i$  and a receiver of type  $j$ . Indeed, it is for example possible that a high frequency source and a low frequency receiver are unable to interact with one another and therefore cannot form a full-fledged sonar system. Besides, we write  $\Xi_\omega \subseteq \Xi$  the set of (functional) sonar systems forming a network  $\omega \in \Omega$ .

Concerning the evaluation of the performance of a given network  $\omega \in \Omega$ , let  $P_d^\omega(t)$  be the probability of cumulative detection of a target  $t \in T$  by  $\omega$  and  $P_d^{(s,r)}(t)$  the probability of instantaneous detection of a target  $t \in T$  by a sonar system  $(s, r) \in \Xi_\omega$ . The calculation of these detection probabilities is further described in subsection 2.1.2. As such, a target is said to be covered (or detected) when the cumulative detection probability exceeds a certain threshold  $\phi \in [0, 1]$  set upstream and generally close to 1 (e.g. 0.95), as done in [25]. More precisely, it corresponds to the concept of cooperative binary coverage [20, 39] (“all or nothing”), also known as cooperative cover [5, 49], although the individual contributions of the sonar systems are based on a gradual (or partial) coverage through a detection model with a decay function (e.g. Fermi). In other words, once the individual contributions have been aggregated, either the detection takes place, or it does not. This is in contrast to its counterpart, the cooperative gradual coverage [20, 39], or joint partial coverage [49], where there may not be detection in the strict sense defined previously, but where partial detection is nevertheless accounted for (after aggregating individual contributions).

The objective (cost) function we will use here captures the coverage rate of the AoI by some network  $\omega \in \Omega$ , or, in other words, the proportion of targets covered. It is explicitly defined as

$$f: \Omega \rightarrow [0, 1]$$

$$\omega \mapsto \frac{1}{|T|} \sum_{t \in T} \sigma(P_d^\omega(t)), \quad (11)$$

where

$$\sigma(x) = \begin{cases} 1 & \text{if } x \geq \phi, \\ 0 & \text{otherwise.} \end{cases} \quad (12)$$

Note that it is possible to weight the different targets and, by extension, the cells in which they are located to put more or less emphasis on certain areas. This could be useful if one knows the probability distribution of the target’s presence in a particular area or if one wishes to protect certain key sites such as docks, straits, harbor basins, anchored ships or even

harbor entrances as discussed in [18, 19, 52]. However, for ease of use, we consider unitary weights in this paper, without this choice being restrictive<sup>4</sup>.

Finally, we look for the optimal solution (network)  $\omega^* \in \Omega$ , i.e. the one maximizing the newly-defined objective function  $f$ :

$$\omega^* = \arg \max_{\omega \in \Omega} f(\omega). \quad (13)$$

### 2.1.2. Multistatic Detection Theory

*Active sonar equation and Cassini ovals.* By rearranging the terms of the active sonar equation presented in [59], it is possible to express the Transmission Losses (TLs) as a function of other terms such as Source Level (SL), Noise Level (NL), Target Strength (TS), Detection Threshold (DT) and the Directivity Index (DI) of the receiving antenna (units: dB). Note that this is true for the noise-limited case (the one examined here), but also for the reverberation-limited case (not examined). The TLs include geometric and absorption losses based on the source-to-target distance  $d_{s,t}$  and the target-to-receiver distance  $d_{t,r}$ . Neglecting absorption losses, one may derive the equation

$$d_{s,t}d_{t,r} = \rho_0^2, \quad (14)$$

where  $\rho_0 \in \mathbb{R}^+$ , called the ‘‘Range of the Day (RoD)’’<sup>5</sup> [21, 51], encompasses all of the above-mentioned terms (except TLs) and corresponds to the distance at which the detection probability is 50 % for a sonar system in monostatic configuration and in a given environment [21]<sup>6</sup>. In other words, this translates to the maximum allowed transmission losses to have this 50 % detection probability. Then, relative to this  $\rho_0$ , if the target is further away (higher losses), then the detection probability is lower, and if the target is closer (lower losses), then the detection probability is higher. Note that this detection probability of 50 % is an arbitrary convention which has a direct influence on the DT value (embedded within  $\rho_0$ ). Indeed, by setting a detection probability (e.g. 0.5) and a false alarm probability (e.g.  $10^{-4}$ ), then it is possible to derive a value for DT (under a certain statistical distribution for NL) so as to obtain these respective detection and false alarm ratios [10, 59]. Hence, some could have chosen different values for the detection probability (e.g. 0.9) and the false alarm probability (e.g.  $10^{-6}$ ), which would have led to a different DT value and therefore a lower

---

<sup>4</sup>Indeed, apart from the weights associated with the targets in the objective function, the rest of the formulations remain unaltered.

<sup>5</sup>In the literature, we also find ‘‘range of the moment’’ [1] and  $r_{50}$  [2, 42] as synonyms for RoD.

<sup>6</sup>For a sonar system in monostatic configuration, this equation becomes  $d = \rho_0$  where  $d$  is the distance from the target.

or higher  $\rho_0$  value with a different interpretation. In other respects, the advantage of neglecting absorption losses to obtain this equation is that it gives us a visual interpretation of the geometric locus where the detection probability is greater than or equal to 0.5 for a given sonar system. This geometric interpretation is otherwise known as Cassini ovals in the literature [11, 37, 48] and translates graphically into an isocontour where the detection probability is 0.5 (by convention). A visualization of these ovals is available in Figure 3 and first row of Figure 4. Ex post facto corrections are possible to reintegrate absorption losses, as proposed in [21].

For a sonar system in bistatic configuration, we introduce the distance in monostatic equivalent [21] defined as

$$\rho_{t,s,r} = \sqrt{d_{s,t}d_{t,r}}. \quad (15)$$

This will allow us to derive detection models in the monostatic case and to refer to them when we have a sonar system in bistatic configuration since we then have

$$\rho_{t,s,r} = \rho_0, \quad (16)$$

which corresponds to the equation of a sonar system in monostatic configuration.

*Instantaneous detection probability.* As it is the case in the literature related to WSNs [17, 40], we distinguish two main categories of detection (sensing) models: deterministic (binary) and probabilistic (diffuse). We briefly present the two classes to express this instantaneous detection probability, also known as the single-ping probability [22].

The deterministic model, also known as Cookie-Cutter or Definite-Range [15, 21, 25] in the MSN-specific literature; is formally defined as

$$P_d^{(s,r)}(t) = \begin{cases} 1 & \text{if } \rho_{t,s,r} \leq \rho_0, \\ 0 & \text{otherwise.} \end{cases} \quad (17)$$

This can be interpreted as the best case scenario, i.e. systematic detection within the Cassini oval. Concerning probabilistic models, several so-called ideal models (because monotonic decreasing<sup>7</sup>) have been proposed in the literature [21, 23], including an exponential function and a class of parameterizable functions called Fermi, related to the Fermi–Dirac distribution [46]. The common denominator of these probabilistic models is a

---

<sup>7</sup>In practice, there can be sudden drops in detection due to the particular propagation of acoustic waves underwater.

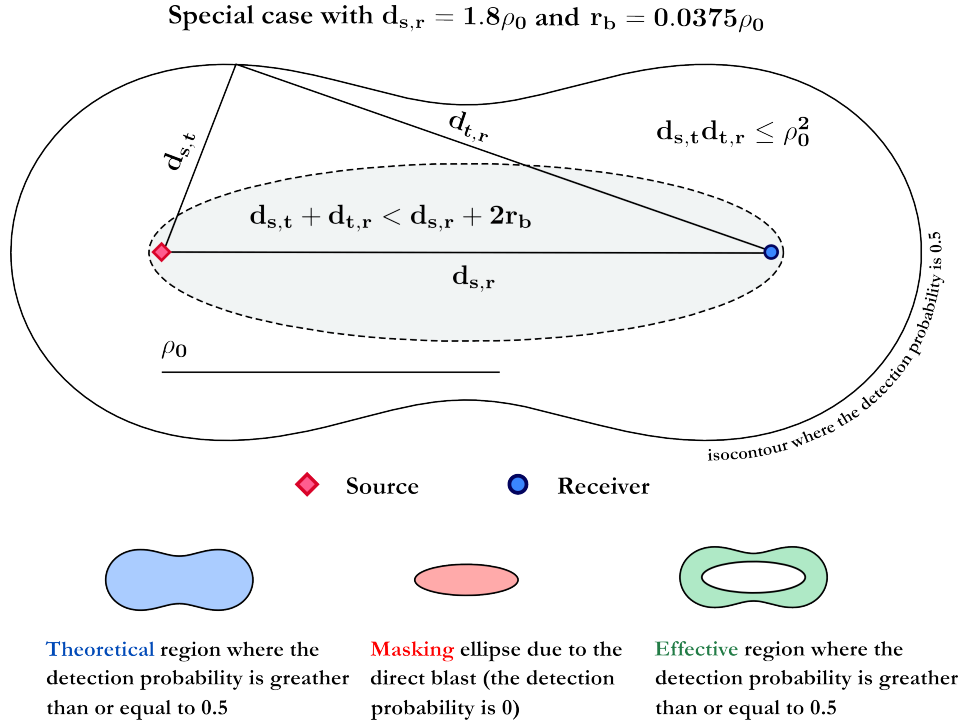


Figure 3: Theory of multistatic detection: a simplified view through Cassini ovals.

detection probability of 50 % when  $\frac{\rho_{t,s,r}}{\rho_0} = 1$ , in order to be consistent with the definition of the RoD introduced above as described in [21]. We recall here the equation governing this class of Fermi functions, a special case of sigmoid/logistic function and defined as

$$P_d^{(s,r)}(t) = \frac{1}{1 + 10^{\frac{\left(\frac{\rho_{t,s,r}}{\rho_0}\right)^{-1}}{b}}}, \quad (18)$$

where  $b \in \mathbb{R}^+$  is called the diffusivity parameter and controls the rate of decay of the detection probability as a function of the ratio  $\frac{\rho_{t,s,r}}{\rho_0}$ . Finally, a sample of these detection models may be seen in Figure 4 with different inter-sensor spacings expressed as multiples of the RoD  $\rho_0$ .



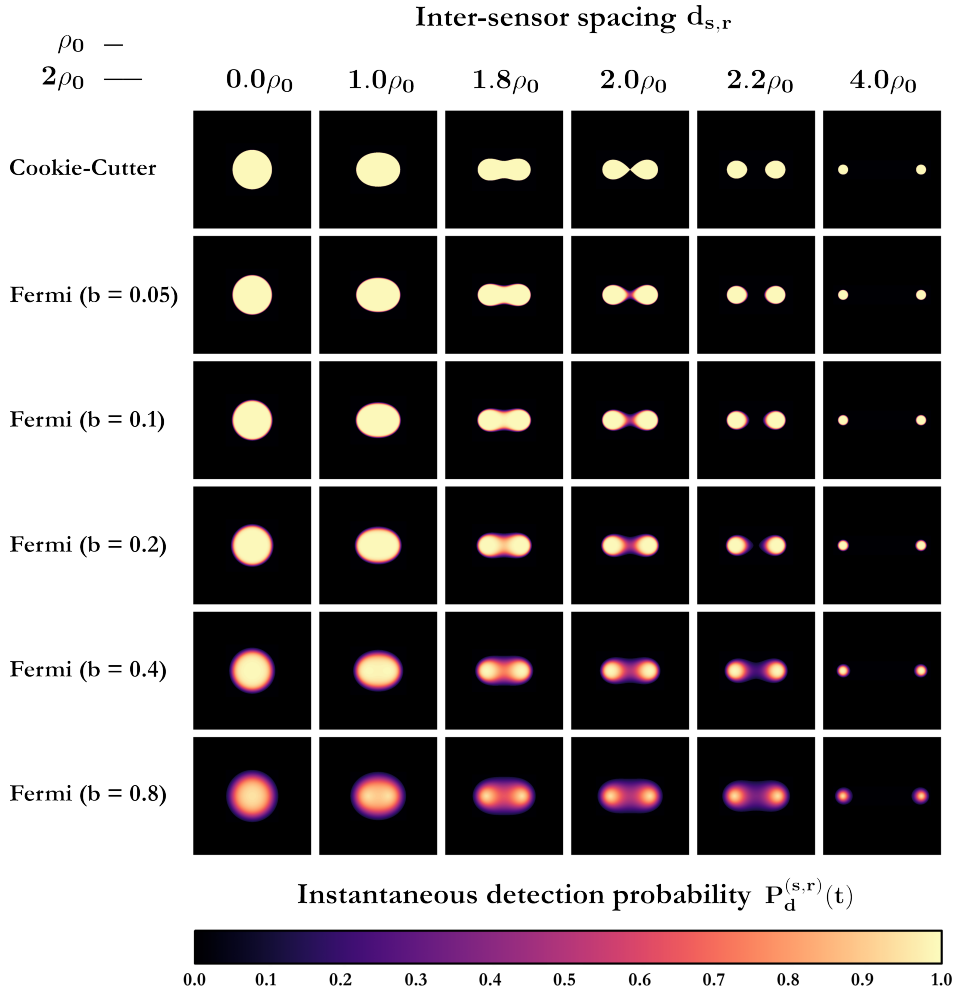


Figure 4: Instantaneous detection probability for a selection of models (deterministic and probabilistic).

*Direct blast effect.* In addition, there is also an adverse effect called direct blast and materialized geometrically by a masking ellipse whose foci are the source and the receiver. Within this ellipse, detection is theoretically not possible [11, 38]. In a nutshell, this happens whenever an echo reaches the receiver while it is still receiving the original signal, and it is therefore unable to process it. The magnitude of this ellipse is proportional to the pulse duration  $\tau \in \mathbb{R}^+$  (in  $s$ ) and the celerity of sound underwater  $c \in \mathbb{R}^+$  (in  $km \cdot s^{-1}$ ). We then define  $r_b = \frac{c\tau}{2}$  (in  $km$ ) which is equal to half the “pulse length”, i.e. the distance traveled by the acoustic wave over the period  $\tau$ . Hence, detection will not be possible if [38, 51]

$$d_{s,t} + d_{t,r} < d_{s,r} + 2r_b. \quad (19)$$

The mathematical details of this equation are discussed in greater depth in Appendix A. Finally, the direct blast effect is illustrated in Figure 5 with different values of  $r_b$  expressed in multiples of  $\rho_0$ , the RoD.

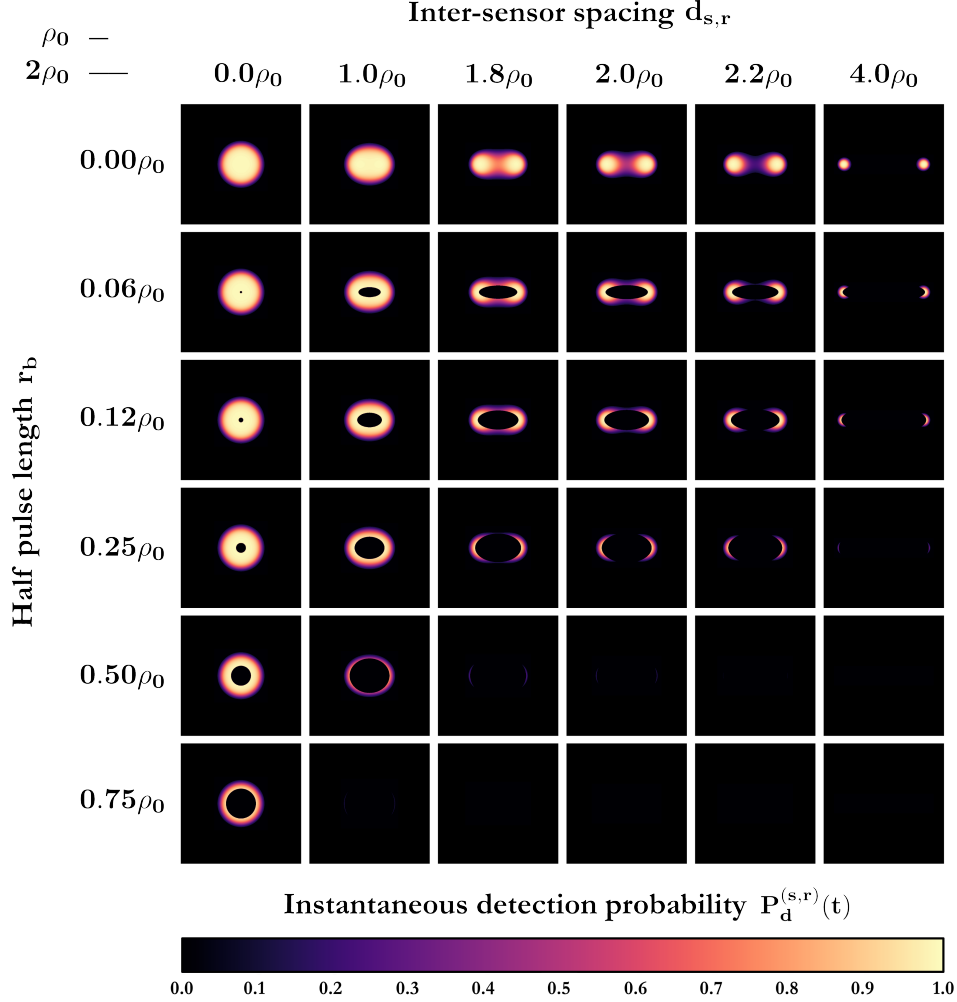


Figure 5: Influence of the direct blast effect on the probabilistic (diffuse) Fermi model with  $b = 0.4$

*Cumulative detection probability.* We first assume that the detections or, more precisely, the ensonifications, are stochastically independent from one another as assumed in [15, 21, 23, 25, 42, 62], although this is partially questioned in [23]. Then, for a sonar system  $\omega \in \Omega$  and a target  $t \in T$ , we introduce

$$P_d^\omega(t) = 1 - \prod_{(s,r) \in \Xi_\omega} \left(1 - P_d^{(s,r)}(t)\right), \quad (20)$$

corresponding to the probability that at least one of the sonar systems detects the target, or, in other words, one minus the probability that none of the sonar systems detects the aforementioned target as done in [23, 25] (called “networked detection probability”). See Figure 6 for an illustration of the computation of cumulative detection probabilities on a sample of basic patterns that may be used, for example, to tile a given space (mainly used in open water and for homogeneous sensors as in [51]).

One way of interpreting this cumulative detection probability is to assume that at a given instant, all sources send out sound pulses whose respective reflections will be assessed by the different receivers throughout the area [32]. Indeed, since we are neglecting any temporal dimension here, it therefore corresponds to a snapshot of the overall situation (sort of ideal scenario). Note that it is possible to generalize the above formula by calculating the probability that at least  $K \in \mathbb{N}^+$  sonar systems will detect a given target. This gives us

$$P_d^\omega(t) = \sum_{k \in \llbracket K, |\Xi_\omega| \rrbracket} \sum_{\Xi' \in \mathcal{P}_k(\Xi_\omega)} \left( \prod_{(s,r) \in \Xi'} P_d^{(s,r)}(t) \prod_{(s,r) \in \Xi_\omega \setminus \Xi'} (1 - P_d^{(s,r)}(t)) \right), \quad (21)$$

where the notation  $\mathcal{P}_k(\Xi_\omega)$  corresponds to the set of subsets of  $\Xi_\omega$  with cardinality  $k$  (i.e. subsets with  $k$  sonar systems from the power set), formally defined by  $\mathcal{P}_k(\Xi_\omega) = \{X \subseteq \Xi_\omega \mid |X| = k\}$ . A more condensed formula can be derived by replacing the two outer sums by a single sum iterating over  $\mathcal{P}_{\geq K}(\Xi_\omega) = \{X \subseteq \Xi_\omega \mid |X| \geq K\}$ , i.e. all subsets with cardinality greater than or equal to  $K$ . In order to minimize the number of calculations performed (frugality-driven), when  $K \geq \frac{(|\Xi_\omega|+1)}{2}$ , the cumulative detection probability is computed using equation (21), whereas when  $K < \frac{(|\Xi_\omega|+1)}{2}$ , the cumulative detection probability is computed as follows:

$$P_d^\omega(t) = 1 - \sum_{k \in \llbracket 0, K-1 \rrbracket} \sum_{\Xi' \in \mathcal{P}_k(\Xi_\omega)} \left( \prod_{(s,r) \in \Xi'} P_d^{(s,r)}(t) \prod_{(s,r) \in \Xi_\omega \setminus \Xi'} (1 - P_d^{(s,r)}(t)) \right). \quad (22)$$

Whenever  $K = 1$ , with this last equation 22, we do indeed fall back on equation 20 ( $P_0(\Xi_\omega) = \emptyset$ ) which is then a special case.

*Coastlines.* As for the coastlines, it is simply a matter of drawing two segments, one between the source and the target and the other between the target and the receiver. Then, using image synthesis algorithms such as the ones described in [3, 7], it is possible to discretize each of these two segments and determine if there is a collision with one of the terrestrial cells of the

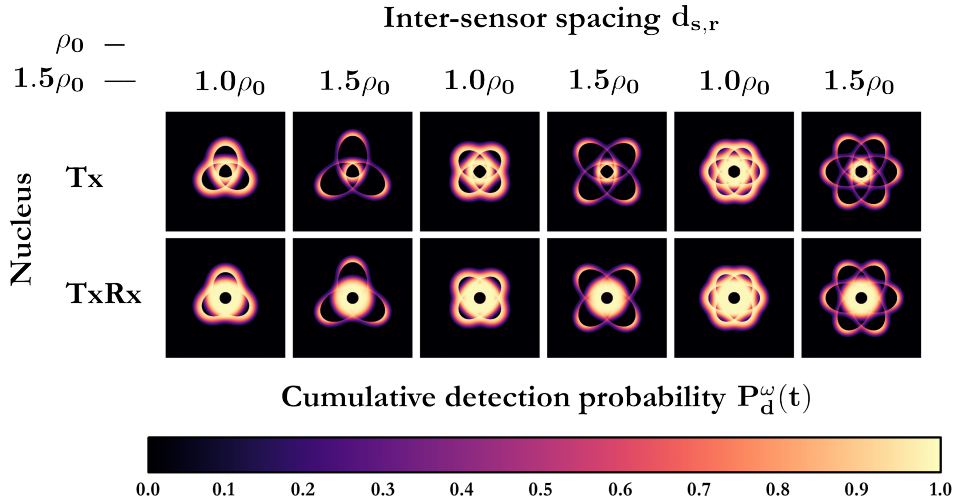


Figure 6: Cumulative detection probability on the three basic tessellation shapes (triangle, square and hexagon). Fermi model with  $b = 0.4$  and  $r_b = 0.5\rho_0$ . One Rx buoy at each pole and two configurations for the nucleus: Tx (top line) and TxRx (bottom line).

grid. If there is a collision on one of the two segments, then we set the instantaneous detection probability to zero. Note that the accuracy of such an action will thus depend directly on the the granularity of the working grid. Finally, this approach remains reasonable, as we are operating on restricted areas (in terms of longitude/latitude extent) where the impact of the earth’s rotundity may be neglected. Indeed, over a restricted area, a straight line on a map projection is virtually identical to the great-circle route, i.e. “straight” line on the globe or shortest distance between two points.

*Heterogeneous sensors.* To generalize the current considerations to the case of heterogeneous sensors, we have chosen to extend the definition of the RoD so that it now depends on both the type of source and the type of receiver comprising a given sonar system. Thus, we introduce  $\rho_0^{i,j} \in \mathbb{R}^+$  as the RoD of the sonar system resulting from the pairing of a source of type  $i \in I$  with a receiver of type  $j \in J$  if the latter two are mutually compatible, i.e.  $(i, j) \in C$ . All that has been developed beforehand remains unaltered with this definition enlargement.

### 2.1.3. Core Linearization

First of all, let us recall that a target  $t \in T$  is considered as detected by the network  $\omega \in \Omega$  when the cumulative detection probability  $P_d^\omega(t)$  is higher than the detection threshold  $\phi$ , i.e. whenever

$$1 - \overbrace{\prod_{(s,r) \in \Xi_\omega} \left(1 - P_d^{(s,r)}(t)\right)}^{P_d^\omega(t)} \geq \phi. \quad (23)$$

Then, by linearizing the previous expression through the logarithm as done in [25], one obtains

$$\sum_{(s,r) \in \Xi_\omega} \underbrace{\log_{(1-\phi)} \left(1 - P_d^{(s,r)}(t)\right)}_{\tilde{P}_d^{(s,r)}(t)} \geq 1, \quad (24)$$

where  $\tilde{P}_d^{(s,r)}(t)$  is then defined as the individual contribution of the sonar system  $(s, r) \in \Xi_\omega$  in the detection of the target  $t \in T$  and  $\tilde{P}_d^\omega(t)$  is the total contribution of the network  $\omega$  in the detection of the target  $t$ .

Finally, in order to lighten the model and without loss of generality, we do not take into account the contributions where the instantaneous detection probability is lower than a threshold  $\epsilon \simeq 0$ . Equivalently, taking into account the newly defined individual contributions and considering a target  $t \in T$ , a sonar system  $(s, r) \in \Xi$  will be discarded if

$$\tilde{P}_d^{(s,r)}(t) < \tilde{\epsilon}, \quad (25)$$

where  $\tilde{\epsilon} = \log_{(1-\phi)}(1 - \epsilon)$  is an enforced minimal contribution threshold.

## 2.2. Base Models

We begin by giving the two most intuitive models for solving the problem at hand, which we will subsequently refer to as the base (naïve) models.

*Model  $M_1$ .* Concerning the decision variables, we first have  $s_e^i \in \{0, 1\}$  where  $s_e^i = 1$  if a source of type  $i \in I$  is deployed on position  $e \in E$  (0 otherwise) and  $r_e^j \in \{0, 1\}$  where  $r_e^j = 1$  if a receiver of type  $j \in J$  is deployed on position  $e \in E$ . Then, we have the variable  $x_t \in \{0, 1\}$  where  $x_t = 1$  if the target  $t \in T$  is covered (0 otherwise).

Furthermore, for the two base models, we introduce an auxiliary binary variable  $y_{e,e'}^{i,j} \in \{0, 1\}$  where  $y_{e,e'}^{i,j} = 1$  if a source of type  $i \in I$  is deployed on position  $e \in E$  and if a receiver of type  $j \in J$  is deployed on position  $e' \in E$ . This auxiliary variable is formally defined as:

$$y_{e,e'}^{i,j} = s_e^i r_{e'}^j, \quad \forall e \in E, i \in I, e' \in E, j \in J. \quad (26)$$

Finally, the first model  $M_1$  is written as follows:

$$\max. \frac{1}{|T|} \sum_{t \in T} x_t \quad (27)$$

$$\text{s.t.} \sum_{e \in E} \sum_{i \in I} \sum_{e' \in E} \sum_{j \in J} \tilde{P}_d^{((e,i),(e',j))}(t) y_{e,e'}^{i,j} \geq x_t \quad \forall t \in T \quad (28)$$

$$\begin{aligned} & \substack{(i,j) \in C \\ \tilde{P}_d^{((e,i),(e',j))}(t) \geq \bar{\epsilon} \\ (e=e' \wedge i=j) \vee e \neq e'} \end{aligned}$$

$$y_{e,e'}^{i,j} \leq s_e^i \quad \forall e \in E, \forall i \in I, \forall e' \in E, \forall j \in J \quad (29)$$

$$y_{e,e'}^{i,j} \leq r_{e'}^j \quad \forall e \in E, \forall i \in I, \forall e' \in E, \forall j \in J \quad (30)$$

$$\sum_{e \in E} s_e^i \leq n_{Tx}^i \quad \forall i \in Tx \quad (31)$$

$$\sum_{e \in E} r_e^i \leq n_{Rx}^i \quad \forall i \in Rx \quad (32)$$

$$\sum_{e \in E} s_e^i \leq n_{TxRx}^i \quad \forall i \in TxRx \quad (33)$$

$$s_e^i = r_e^i \quad \forall e \in E, \forall i \in TxRx \quad (34)$$

$$\sum_{i \in Tx} s_e^i + \sum_{i \in Rx} r_e^i + \sum_{i \in TxRx} s_e^i \leq 1 \quad \forall e \in E \quad (35)$$

$$x_t \in \{0, 1\} \quad \forall t \in T \quad (36)$$

$$s_e^i \in \{0, 1\} \quad \forall e \in E, \forall i \in I \quad (37)$$

$$r_{e'}^j \in \{0, 1\} \quad \forall e \in E, \forall j \in J \quad (38)$$

$$y_{e,e'}^{i,j} \in \{0, 1\} \quad \forall e \in E, \forall i \in I, \forall e' \in E, \forall j \in J \quad (39)$$

In this model, constraint (28) accounts for contributions from existing sonar systems only, i.e., whenever  $y_{e,e'}^{i,j} = 1$  or, in other words, when  $s_e^i = 1$  and  $r_{e'}^j = 1$  for a given source  $(e, i) \in E \times I$  and a given receiver  $(e', j) \in E \times J$ . Note that the constraint  $(e = e' \wedge i = j) \vee e \neq e'$  implies that

- if  $e = e'$ , then necessarily we are dealing with a TxRx buoy (hence we require  $i = j$ ), otherwise,
- if  $e \neq e'$ , there are no restrictions, i.e. it is possible to consider any pair of buoys (the objective is to avoid considering impossible cases and to lighten the model).

The constraints (29) and (30) are the linearization constraints of the auxiliary variable  $y_{e,e'}^{i,j}$ . Constraints (31), (32) and (33) restrict the number of transmitter-only buoys (Tx), the number of receiver-only buoys (Rx) and the number of transmitter-receiver buoys (TxRx) respectively. Constraint (34) compels the deployment of the source and receiver of the same TxRx buoy, since one cannot be deployed without the other: it is the same buoy. Constraint (35) is a deployment constraint limiting to one and only one buoy per position. Finally, constraints (36), (37), (38) and (39) are the integrity constraints of the different variables.

Model  $M_2$ . Substituting the equations (29) and (30) by

$$2y_{e,e'}^{i,j} \leq s_e^i + r_{e'}^j \quad (40)$$

yields the second base model denoted  $M_2$ .

### 2.3. Improved models: extended linearization of Oral & Kettani

For the improved models, we rely on the linearization procedure named OK1 in [25] and initially proposed by Oral and Kettani in [50] to linearize quadratic formulations. This linearization is extended for the case of heterogeneous sensors and 7 different models are thus derived, all with their own specificities, either on aggregations or on the choice of auxiliary variables. Addressed problem aside (new in the literature), this is one of the major contributions of this paper. Moreover, as proposed in [25], the collection of models hereafter are available in two variants depending on the aggregation of the individual contributions (with respect to the sources or with respect to the receivers) giving us an effective total of 16 models. A complete example will be given for the first model  $M_3$ .

#### 2.3.1. Model $M_3$

We begin here by considering the variant denoted -S in which the aggregation of individual contributions is done by fixing a target  $t \in T$  and a source of type  $i \in I$  on position  $e \in E$  as follows:

$$L_{e,i,t} = \sum_{\substack{e' \in E \\ (i,j) \in C \\ \tilde{P}_d^{((e,i),(e',j))}(t) \geq \tilde{\epsilon} \\ (e=e' \wedge i=j) \vee e \neq e'}} \sum_{j \in J} \tilde{P}_d^{((e,i),(e',j))}(t). \quad (41)$$

We also introduce an auxiliary variable  $z_{e,i,t} \in \mathbb{R}^+$  that can be formally defined as

$$z_{e,i,t} = \begin{cases} L_{e,i,t} - \sum_{\substack{e' \in E \\ (i,j) \in C \\ \tilde{P}_d^{((e,i),(e',j))}(t) \geq \tilde{\epsilon} \\ (e=e' \wedge i=j) \vee e \neq e'}} \sum_{j \in J} \tilde{P}_d^{((e,i),(e',j))}(t)r_{e'}^j & \text{if } s_e^i = 1, \\ 0 & \text{otherwise.} \end{cases} \quad (42)$$

The M3-S model is therefore written as follows:

max. (27)

s.t. (31), (32), (33), (34), (35)

$$\sum_{e \in E} \left( \sum_{i \in I} L_{e,i,t} s_e^i - z_{e,i,t} \right) \geq x_t \quad \forall t \in T \quad (43)$$

$$z_{e,i,t} \geq L_{e,i,t} s_e^i - \sum_{\substack{e' \in E \\ (i,j) \in C \\ \tilde{P}_d^{((e,i),(e',j))}(t) \geq \tilde{\epsilon} \\ (e=e' \wedge i=j) \vee e \neq e'}} \sum_{j \in J} \tilde{P}_d^{((e,i),(e',j))}(t) r_{e'}^j \quad \forall e \in E, \forall i \in I, \forall t \in T \quad (44)$$

(36), (37), (38)

$$z_{e,i,t} \in \mathbb{R}^+ \quad \forall e \in E, \forall i \in I, \forall t \in T \quad (45)$$

Here, constraints (43) and (44) replace constraints (28), (29), and (30) of model  $M_1$ . To understand this model, it is necessary to distinguish the following two cases:

- In the first case, assume that  $s_e^i = 0$  for a source of type  $i \in I$  on position  $e \in E$ . With  $s_e^i = 0$  and knowing that we want to maximize  $-z_{e,i,t}$  in (43), it is therefore the same as minimizing  $z_{e,i,t}$ . Yet,  $z_{e,i,t}$  is lower bounded by  $-\sum_{e' \in E} \sum_{j \in J} \tilde{P}_d^{((e,i),(e',j))}(t) r_{e'}^j$  in (44), which thus

constrains  $z_{e,i,t} = 0$  by (45). This is correct, because no contribution involving a sonar system constituted with the source  $s_e^i$  is accounted for, the latter not being deployed.

- In the second case, suppose that  $s_e^i = 1$  for a source of type  $i \in I$  on position  $e \in E$ . In (44),  $z_{e,i,t}$  is lower bounded by  $L_{e,i,t} - \sum_{e' \in E} \sum_{j \in J} \tilde{P}_d^{((e,i),(e',j))}(t) r_{e'}^j$ . However, knowing that we want to

minimize  $z_{e,i,t}$  in (43), we thus obtain  $z_{e,i,t} = L_{e,i,t} - \sum_{e' \in E} \sum_{j \in J} \tilde{P}_d^{((e,i),(e',j))}(t) r_{e'}^j$ .

Finally, the terms  $L_{e,i,t}$  cancel out in (43) and we eventually get  $\sum_{e' \in E} \sum_{j \in J} \tilde{P}_d^{((e,i),(e',j))}(t) r_{e'}^j$ , which is equivalent to accounting for

all contributions such that  $s_e^i r_{e'}^j = 1$ , which is correct. A graphical illustration of this case is presented in Figure 7 to help the reader understand the global picture.



We will now present the -R variant of this same model. In this variant, the aggregation of individual contributions is done by fixing a target  $t \in T$  and a receiver of type  $j \in J$  on position  $e \in E$  as follows:

$$L_{e',j,t} = \sum_{\substack{e \in E \\ (i,j) \in C \\ \tilde{P}_d^{((e,i),(e',j))}(t) \geq \bar{\epsilon} \\ (e=e' \wedge i=j) \vee e \neq e'}} \sum_{i \in I} \tilde{P}_d^{((e,i),(e',j))}(t) \quad (46)$$

The M3-R model is then formulated as follows:

max. (27)

s.t. (31), (32), (33), (34), (35)

$$\sum_{e' \in E} \left( \sum_{j \in J} L_{e',j,t} r_{e'}^j - z_{e',j,t} \right) \geq x_t \quad \forall t \in T \quad (47)$$

$$z_{e',j,t} \geq L_{e',j,t} r_{e'}^j - \sum_{\substack{e \in E \\ (i,j) \in C \\ \tilde{P}_d^{((e,i),(e',j))}(t) \geq \bar{\epsilon} \\ (e=e' \wedge i=j) \vee e \neq e'}} \sum_{i \in I} \tilde{P}_d^{((e,i),(e',j))}(t) s_e^i \quad \forall e' \in E, \forall j \in J, \forall t \in T \quad (48)$$

(36), (37), (38)

$$z_{e',j,t} \in \mathbb{R}^+$$

$$\forall e' \in E, \forall j \in J, \forall t \in T \quad (49)$$

The reasoning is strictly analogous to the -S variant presented above.

We have therefore implemented the -R variant for the upcoming 7 models, but on the basis of numerous preliminary experiments, we have come to the same conclusion as Fügenschuh et al. [25]: -S variants tend to be more efficient than -R variants. One possible explanation is that there are usually more receivers than sources, the latter being of lower cost. Aggregation by fixing a source is therefore a priori more advantageous, at least for these formulations. Hence, for the following, when we refer to model  $M_i$ ,  $\forall i \in \llbracket 3, 9 \rrbracket$ , this means that we consider the -S variant by default. Besides, for reasons of parsimony, from now onwards we will only give the -S variant for each of these models knowing that we will present the experiments only for these variants.

### 2.3.2. Model $M_4$

The  $M_4$  model is very similar to the  $M_3$  model. Indeed, we substitute the auxiliary variable  $z_{e,i,t} \in \mathbb{R}^+$  by the auxiliary variable  $z_{e,t} \in \mathbb{R}^+$ . This closely related model takes advantage of the fact that only one source can be deployed on a given deployment position. It is written as follows for the -S variant:

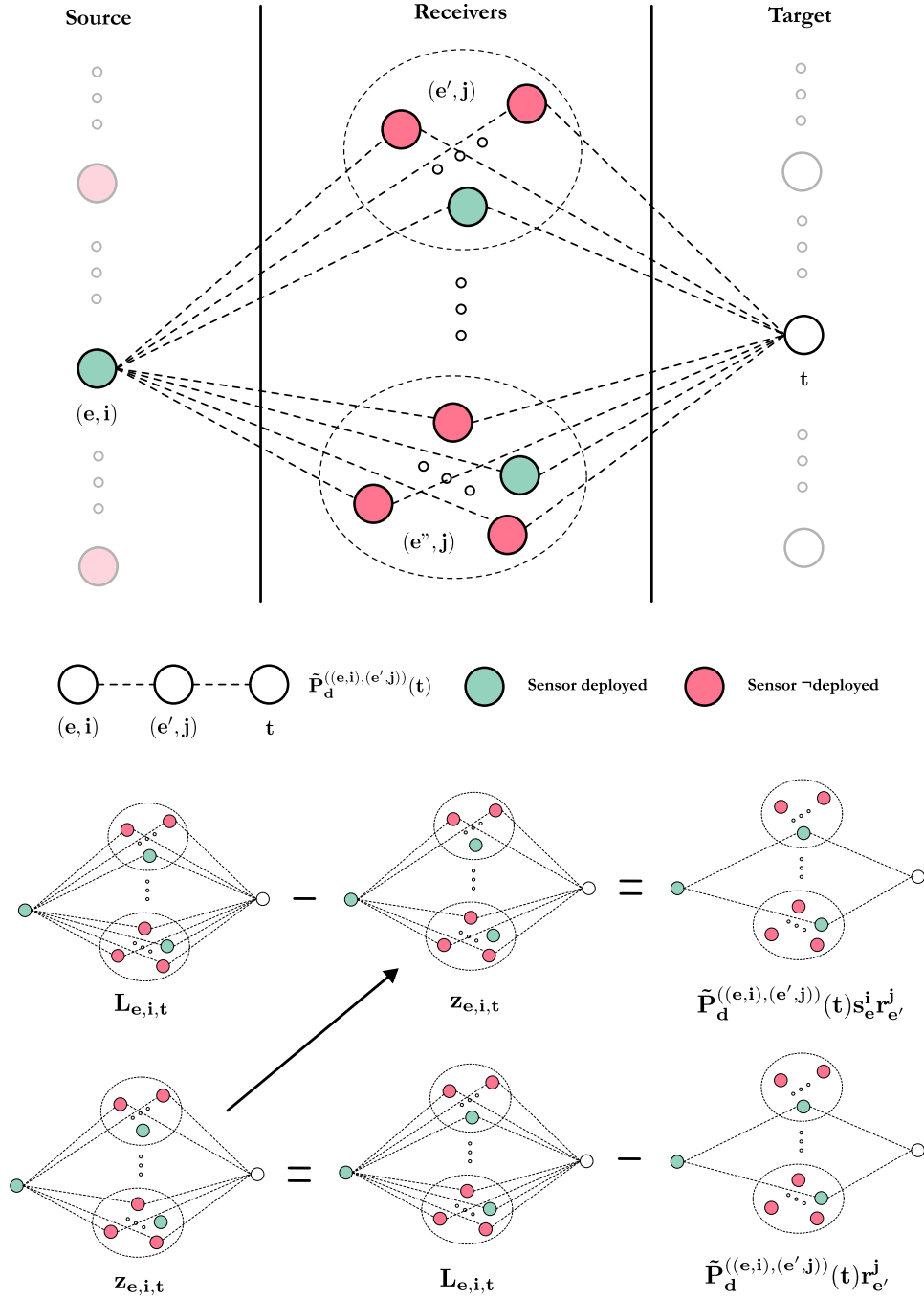


Figure 7: Model  $M_3-S$ : illustration of case  $n^2$  where  $s_{e,i} = 1$  for a given source  $(e, i) \in E \times I$  and target  $t \in T$ .

max. (27)

s.t. (31), (32), (33), (34), (35)

$$\sum_{e \in E} \left( \sum_{i \in I} L_{e,i,t} s_e^i \right) - z_{e,t} \geq x_t \quad \forall t \in T \quad (50)$$

$$z_{e,t} \geq L_{e,i,t} s_e^i - \sum_{\substack{e' \in E \\ (i,j) \in C \\ \tilde{P}_d^{((e,i),(e',j))}(t) \geq \bar{\epsilon} \\ (e=e' \wedge i=j) \vee e \neq e'}} \sum_{j \in J} \tilde{P}_d^{((e,i),(e',j))}(t) r_{e'}^j \quad \forall e \in E, \forall i \in I, \forall t \in T \quad (51)$$

(36), (37), (38)

$$z_{e,t} \in \mathbb{R}^+ \quad \forall e \in E, \forall i \in I, \forall t \in T \quad (52)$$

If no source is deployed on position  $e \in E$ , then  $z_{e,t}$  will be set to 0 by (50), (51) and (52) as in the previous model since we will try to minimize it. On the other hand, if a source of type  $i \in I$  is deployed on position  $e \in E$  ( $s_e^i = 1$ ), then the variable  $z_{e,t}$  will be set to  $L_{e,i,t} - \sum_{\substack{e' \in E \\ (i,j) \in C \\ \tilde{P}_d^{((e,i),(e',j))}(t) \geq \bar{\epsilon} \\ (e=e' \wedge i=j) \vee e \neq e'}} \sum_{j \in J} \tilde{P}_d^{((e,i),(e',j))}(t) r_{e'}^j$  by (51), this constraint acting as a maximum.

Then the terms will cancel each other out in 50, leaving us only with individual contributions such as  $s_e^i r_{e'}^j = 1$ , which is correct.

### 2.3.3. Model $M_5$

In the sequel, we will aggregate the contributions at a higher level by fixing a target  $t \in T$  and a position  $e \in E$  (which can accommodate a source) as follows:

$$L_{e,t} = \sum_{i \in I} \sum_{e' \in E} \sum_{\substack{j \in J \\ (i,j) \in C \\ \tilde{P}_d^{((e,i),(e',j))}(t) \geq \bar{\epsilon} \\ (e=e' \wedge i=j) \vee e \neq e'}} \tilde{P}_d^{((e,i),(e',j))}(t) = \sum_{i \in I} L_{e,i,t} \quad (53)$$

It is important to note that it will be possible to use the aggregations  $L_{e,i,t}$  to compute  $L_{e,t}$ , this will be particularly useful for the forthcoming models  $M_7$ ,  $M_8$  and  $M_9$  in a pursuit of computational efficiency. We also introduce a new auxiliary meta-variable  $s_e \in \{0, 1\}$  where  $s_e = 1$  if a source has been deployed on position  $e \in E$  (regardless of the type). The M5-S model is therefore written as:

max. (27)

s.t. (31), (32), (33), (34), (35)

$$\sum_{e \in E} \left( L_{e,t} s_e - \sum_{i \in I} z_{e,i,t} \right) \geq x_t \quad \forall t \in T \quad (54)$$

$$z_{e,i,t} \geq L_{e,t} s_e^i - \sum_{\substack{e' \in E \\ (i,j) \in C \\ \tilde{P}_d^{((e,i),(e',j))}(t) \geq \bar{\epsilon} \\ (e=e' \wedge i=j) \vee e \neq e'}} \sum_{j \in J} \tilde{P}_d^{((e,i),(e',j))}(t) r_{e'}^j \quad \forall e \in E, \forall i \in I, \forall t \in T \quad (55)$$

$$s_e = \sum_{i \in I} s_e^i \quad \forall e \in E \quad (56)$$

(36), (37), (38)

$$s_e \in \{0, 1\} \quad \forall e \in E \quad (57)$$

$$z_{e,i,t} \in \mathbb{R}^+ \quad \forall e \in E, \forall i \in I, \forall t \in T \quad (58)$$

First, constraint 56 is used to find out whether a source has been deployed on position  $e \in E$ . Then, the idea remains the same. If no source is deployed on position  $e \in E$ , then all  $z_{e,i,t}$  are set to 0 by (55) and (58). In the opposite case, if a source has been deployed on position  $e \in E$ , then all  $z_{e,i,t}$  except one will be fixed to 0, the latter being fixed to  $L_{e,t} - \sum_{e' \in E} \sum_{j \in J} \tilde{P}_d^{((e,i),(e',j))}(t) r_{e'}^j$  by (55). Eventually, the terms will cancel out in (54) and we will be left with only the valid individual contributions, i.e. whenever  $s_e^i r_{e'}^j = 1$ .

#### 2.3.4. Model $M_6$

This M6 model is very close to the previous one and uses the same principle as the M4 model by substituting  $z_{e,i,t}$  with  $z_{e,t}$ . It is written as follows:

max. (27)

s.t. (31), (32), (33), (34), (35)

$$\sum_{e \in E} (L_{e,t} s_e - z_{e,t}) \geq x_t \quad \forall t \in T \quad (59)$$

$$z_{e,t} \geq L_{e,t} s_e^i - \sum_{\substack{e' \in E \\ (i,j) \in C \\ \tilde{P}_d^{((e,i),(e',j))}(t) \geq \bar{\epsilon} \\ (e=e' \wedge i=j) \vee e \neq e'}} \sum_{j \in J} \tilde{P}_d^{((e,i),(e',j))}(t) r_{e'}^j \quad \forall e \in E, \forall i \in I, \forall t \in T \quad (60)$$

$$s_e = \sum_{i \in I} s_e^i \quad \forall e \in E \quad (61)$$

(36), (37), (38)

$$s_e \in \{0, 1\} \quad \forall e \in E \quad (62)$$

$$z_{e,t} \in \mathbb{R}^+ \quad \forall e \in E, \forall t \in T \quad (63)$$

### 2.3.5. Model $M_7$

From this point on and for the following three models, we will use both aggregations  $L_{e,i,t}$  and  $L_{e,t}$  simultaneously. For this M7 model, we will use only the auxiliary variable  $z_{e,i,t} \in \mathbb{R}^+$ . The M7-S model is written as follows:

max. (27)

s.t. (31), (32), (33), (34), (35)

$$\sum_{e \in E} \left( L_{e,t} s_e - \sum_{i \in I} z_{e,i,t} \right) \geq x_t \quad \forall t \in T \quad (64)$$

$$z_{e,i,t} \geq L_{e,i,t} s_e^i - \sum_{\substack{e' \in E \\ (i,j) \in C \\ \tilde{P}_d^{((e,i),(e',j))}(t) \geq \bar{\epsilon} \\ (e=e' \wedge i=j) \vee e \neq e'}} \sum_{j \in J} \tilde{P}_d^{((e,i),(e',j))}(t) r_{e'}^j \quad \forall e \in E, \forall i \in I, \forall t \in T \quad (65)$$

$$z_{e,i,t} \geq L_{e,i,t} (1 - s_e^i) - L_{e,i,t} (1 - s_e) \quad \forall e \in E, \forall i \in I, \forall t \in T \quad (66)$$

$$s_e = \sum_{i \in I} s_e^i \quad \forall e \in E \quad (67)$$

(36), (37), (38)

$$s_e \in \{0, 1\} \quad \forall e \in E \quad (68)$$

$$z_{e,i,t} \in \mathbb{R}^+ \quad \forall e \in E, \forall i \in I, \forall t \in T \quad (69)$$

If no source is deployed on position  $e \in E$ , then all variables  $z_{e,i,t}$  are set to 0 by (64), (65) and (66). Otherwise, if a source is deployed on position  $e \in E$ , we must distinguish two cases:

- if a source of type  $i \in I$  is deployed at position  $e$ , then  $z_{e,i,t} = L_{e,i,t} - \sum_{\substack{e' \in E \\ (i,j) \in C \\ \tilde{P}_d^{((e,i),(e',j))}(t) \geq \bar{\epsilon} \\ (e=e' \wedge i=j) \vee e \neq e'}} \sum_{j \in J} \tilde{P}_d^{((e,i),(e',j))}(t) r_{e'}^j$  by (65) ( $z_{e,i,t} \geq 0$  through (66)), and,

- if a source of type  $i \in I$  is not deployed on position  $e$ , then  $z_{e,i,t} = L_{e,i,t}$  by (66).

The terms will thus cancel each other out in (64) to finally give us  $\tilde{P}_d^{((e,i),(e',j))}(t)r_{e'}^j$ , which amounts to taking into account the contributions such that  $s_e^i r_{e'}^j = 1$ .

### 2.3.6. Model M8

In this M8 model we will have the two auxiliary variables  $z_{e,t} \in \mathbb{R}^+$  and  $z_{e,i,t} \in \mathbb{R}^+$  which will be used a bit differently from the previous model. The M8-S model is written as follows:

max. (27)

s.t. (31), (32), (33), (34), (35)

$$\left( \sum_{e \in E} L_{e,t} s_e - z_{e,t} \right) \geq x_t \quad \forall t \in T \quad (70)$$

$$z_{e,t} \geq L_{e,t} s_e - \sum_{i \in I} \left( L_{e,i,t} s_e^i - z_{e,i,t} \right) \quad \forall e \in E, \forall t \in T \quad (71)$$

$$z_{e,i,t} \geq L_{e,i,t} s_e^i - \sum_{\substack{e' \in E \\ (i,j) \in C \\ \tilde{P}_d^{((e,i),(e',j))}(t) \geq \bar{\epsilon} \\ (e=e' \wedge i=j) \vee e \neq e'}} \sum_{j \in J} \tilde{P}_d^{((e,i),(e',j))}(t) r_{e'}^j \quad \forall e \in E, \forall i \in I, \forall t \in T \quad (72)$$

$$s_e = \sum_{i \in I} s_e^i \quad \forall e \in E \quad (73)$$

(36), (37), (38)

$$s_e \in \{0, 1\} \quad \forall e \in E \quad (74)$$

$$z_{e,i,t} \in \mathbb{R}^+ \quad \forall e \in E, \forall i \in I, \forall t \in T \quad (75)$$

$$z_{e,t} \in \mathbb{R}^+ \quad \forall e \in E, \forall t \in T \quad (76)$$

If no source is deployed on position  $e \in E$ , then all variables  $z_{e,i,t}$  and  $z_{e,t}$  are set to 0 as it was the case in the previous models. Else, if a source of type  $i \in I$  is deployed at position  $e \in E$ , then  $z_{e,i,t} = L_{e,i,t} - \sum_{e' \in E} \sum_{j \in J} \tilde{P}_d^{((e,i),(e',j))}(t) r_{e'}^j$  by (72) and  $z_{e,t} = L_{e,t} - (L_{e,i,t} - z_{e,i,t}) = L_{e,t} - \tilde{P}_d^{((e,i),(e',j))}(t) r_{e'}^j$  by (71). Finally, all terms cancel out in (70) and we get only the individual contributions where  $s_e^i r_{e'}^j = 1$ .

### 2.3.7. Model M9

Concerning the last model, the idea is slightly different, we introduce a new auxiliary variable  $z_{e',t} \in \mathbb{R}^+$  in addition to  $z_{e,t} \in \mathbb{R}^+$  and it is written as follows:

max. (27)

s.t. (31), (32), (33), (34), (35)

$$\left( \sum_{e \in E} L_{e,t} s_e - z_{e,t} - z'_{e,t} \right) \geq x_t \quad \forall t \in T \quad (77)$$

$$z_{e,t} \geq L_{e,i,t} s_e^i - \sum_{\substack{e' \in E \\ (i,j) \in C \\ \tilde{P}_d^{((e,i),(e',j))}(t) \geq \bar{\epsilon} \\ (e=e' \wedge i=j) \vee e \neq e'}} \sum_{j \in J} \tilde{P}_d^{((e,i),(e',j))}(t) r_{e'}^j \quad \forall e \in E, \forall i \in I, \forall t \in T \quad (78)$$

$$z'_{e,t} \geq L_{e,t} s_e - \sum_{i \in I} L_{e,i,t} s_e^i \quad \forall e \in E, \forall t \in T \quad (79)$$

$$s_e = \sum_{i \in I} s_e^i \quad \forall e \in E \quad (80)$$

(36), (37), (38)

$$s_e \in \{0, 1\} \quad \forall e \in E \quad (81)$$

$$z_{e,t} \in \mathbb{R}^+ \quad \forall e \in E, \forall t \in T \quad (82)$$

$$z'_{e,t} \in \mathbb{R}^+ \quad \forall e \in E, \forall t \in T \quad (83)$$

If no source is deployed on the position  $e \in E$ , then all variables  $z_{e,t}$  and  $z'_{e,t}$  are set to 0. Otherwise, if a source of type  $i \in I$  is deployed at position  $e \in E$ , then  $z_{e,t} = L_{e,i,t} - \sum_{\substack{e' \in E \\ (i,j) \in C \\ \tilde{P}_d^{((e,i),(e',j))}(t) \geq \bar{\epsilon} \\ (e=e' \wedge i=j) \vee e \neq e'}} \sum_{j \in J} \tilde{P}_d^{((e,i),(e',j))}(t) r_{e'}^j$  by (78)

and  $z'_{e,t} = L_{e,t} - L_{e,i,t}$  by (79). Finally, all these terms cancel out in (77) and we get only the individual contributions where  $s_e^i r_{e'}^j = 1$ .

### 2.3.8. Summary

In Table 1, there is a synoptic summary of the improved models' intrinsic characteristics. These characteristics are given for the -S variants, but the reasoning is identical for the -R variants.

Model	Aggregations	Auxiliary variables	Additional constraints
$M_3$	$L_{e,i,t}$	$z_{e,i,t}$	$ E  \cdot  I  \cdot  T $
$M_4$	$L_{e,i,t}$	$z_{e,t}$	$ E  \cdot  I  \cdot  T $
$M_5$	$L_{e,t}$	$z_{e,i,t}, s_e$	$ E  +  E  \cdot  I  \cdot  T $
$M_6$	$L_{e,t}$	$z_{e,t}, s_e$	$ E  +  E  \cdot  I  \cdot  T $
$M_7$	$L_{e,t}, L_{e,i,t}$	$z_{e,i,t}, s_e$	$ E  + 2( E  \cdot  I  \cdot  T )$
$M_8$	$L_{e,t}, L_{e,i,t}$	$z_{e,t}, z_{e,i,t}, s_e$	$ E  +  E  \cdot  T  +  E  \cdot  I  \cdot  T $
$M_9$	$L_{e,t}, L_{e,i,t}$	$z_{e,t}, z'_{e,t}, s_e$	$ E  \cdot  I  \cdot  T  +  E  \cdot  T $

Table 1: Summary table of improved models' characteristics (-S variant)

Note that, in this paper, we have chosen to extend the OK1 formulation, because it presented the best results in [25]. However, it could have been possible to do the same for the different linearizations presented in the above-mentioned article, such as the Chaovalitwongse–Pardalos–Prokopyev’s linearization (CPP) [8] or the Glover’s linearization (GLO) [27], for example. This would have led to the derivation of many other models.

### 3. Numerical Experiments

In this section, we will showcase the instances on which we conducted the experiments, present the results obtained on the different formulations introduced above, and, finally, provide statistical tests carried out a posteriori in order to analyze these results. These statistical tests are based on the two-stage methodology proposed in [25].

#### 3.1. Instances

Before turning our attention to the numerical results, we first discuss the different instances that were used. First, in Table 2, we list the various non-specified control buoys in each of the categories (Tx, Rx, TxRx) that will be used for the upcoming experiments. Note that HF stands for “High-Frequency” and LF for “Low-Frequency”. Then, in Table 3, we summarize the different RoDs  $\rho_0^{i,j}$  (in km) for all compatible sonar systems  $(i, j) \in C$  that could be encountered<sup>8</sup>. Recall that  $I = TxRx \cup Tx$  and  $J = TxRx \cup Rx$  corresponding respectively to all sources and all receivers.

In a GitHub repository<sup>9</sup>, we provide a breakdown of all the various instances as well as an illustration of the grids and the AoIs from which they originate. Note that from a single regular rectangular grid (i.e., a DEM), 25 instances were derived with different volumes of buoys in each of the respective categories. Note that these instances are also described in Tables F.23, F.24, F.25 and F.26 in Appendix F (one table per group of 25 instances). Moreover, these grids were obtained through a down-sampling<sup>10</sup> process of bathymetric and topographic data made publicly-available by the GEneral Bathymetric Chart of the Oceans (GEBCO) as of 2022 [26]. Finally, the various parameters set for the experiments are summarized in Table 4.

---

<sup>8</sup>These figures are not meant to represent real sonar systems performance but are sufficiently realistic for demonstration purposes.

<sup>9</sup><https://github.com/owein-thuillier/MSN-dataset>

<sup>10</sup>This down-sampling procedure enables us to reduce the resolution of a DEM by aggregating several cells into a single one.



Category	TxRx		Tx		Rx			
Type	$A_{HF}$	$B_{LF}$	$C_{HF}$	$D_{LF}$	$E_{HF}$	$F_{HF}$	$G_{LF}$	$H_{LF}$

Table 2: Details of the different buoys considered for each category (Tx, Rx, TxRx).

J \ I	$A_{HF}$	$E_{HF}$	$F_{HF}$	$B_{LF}$	$G_{LF}$	$H_{LF}$
$A_{HF}$	5.0	4.0	3.5	x	x	x
$C_{HF}$	4.5	3.0	2.5	x	x	x
$B_{LF}$	x	x	x	8.0	7.5	6.5
$D_{LF}$	x	x	x	7.0	6.0	5.5

Table 3: Performance ( $\rho_0^{i,j}$ , in km) of the various sonar systems  $(i, j) \in C$ .

$c$	$\tau$	$r_b$	$\phi$	Fermi ( $b$ )	$\epsilon$
1.5	1	0.75	0.95	0.2	$10^{-6}$

Table 4: Parameters set for the numerical experiments.

### 3.2. Results

All the experiments were conducted on a Debian 11 server (64 bits) with 190 GB of RAM and 2 processors Intel® Xeon® Gold 6258R clocked at 2.70 Ghz (50 cores each). Moreover, all the resolutions were done using IBM ILOG CPLEX 20.1 [35] with default settings, 8 threads in parallel and a computational budget of 7200 seconds (2 hours). The models have been implemented in Julia 1.7.3 [6]. In total, the whole set of experiments involved 900 resolutions (100 instances, 9 formulations) and required 1155 hours of CPU time, or approximately 48 days.

In Tables B.6, B.7, B.8 and B.9 in Appendix B, the following information is systematically reported for each instance:

- computation time (in s) if the optimal solution is found within the computational budget of 2 hours; and,
- relative gap (in %) if the computational budget is reached, i.e.:  $\left(\frac{|z_D - z_P|}{|z_P| + \delta}\right) \cdot 100$  where  $z_P$  is the primal objective bound (the incumbent objective value, or lower bound<sup>11</sup>),  $z_D$  is the dual objective bound (the upper

<sup>11</sup>Best integer (feasible) solution found so far for a maximization problem and typically obtained using heuristics or during the branch-and-bound procedure.

bound<sup>12</sup>) and  $\delta \in \mathbb{R}$  a sufficiently small number (typically  $10^{-10}$  for CPLEX [35]). This relative gap corresponds, in essence<sup>13</sup>, to the definition of  $GAP_{UB}$  given in [43] and is the gap returned natively by CPLEX during the branch-and-bound execution.

For the sake of brevity, these two pieces of information are reported in the same table cell. Indeed, when an optimal solution is found in the given budget, then the gap is 0 and it is not necessary to report it. Hence, for a given formulation  $i \in \llbracket 1, 9 \rrbracket$  and instance  $j \in \llbracket 1, 100 \rrbracket$ , this allows us to define the score  $s_{i,j}$ , or figure of merit, as follows [25]:  $s_{i,j} = \min\{7200, t_{i,j}\} + g_{i,j}$ , where  $t_{i,j}$  is the computation time (in s) and  $g_{i,j}$  the relative gap defined previously. The use of a min is simply to ensure that none of the solve times exceed 7200 s, which can happen in practice as discussed in [25]. Indeed, the solver must finish its current operation before terminating the execution if the computational budget is reached, and the min thus allows to get rid of this artifact.

Then, for a given instance  $j \in \llbracket 1, 100 \rrbracket$ , this newly-defined score enables us to order the different formulations  $i \in \llbracket 1, 9 \rrbracket$  with a rank  $R_{i,j} \in \llbracket 1, 9 \rrbracket$ , 1 being the best position. In case of a tie, the average rank is assigned as mentioned in [9, 24]. For example, if three formulations are competing for place number 3, then the average rank is  $\frac{3+4+5}{3} = 4$ . In particular, these ranks will be used for the non-parametric statistical tests in the next subsection to conduct a thorough qualitative analysis of these raw results.

Note that the best result for each instance is displayed in **bold** and that there may be ties for first place. Moreover, at the bottom of each of these tables, several additional metrics are aggregated for each of the different models. For a given formulation (column) and in order of appearance, we find the number of instances solved, the number of times the formulation performed best, the average rank, the average resolution time and, finally, the average relative gap. Finally, in Table 5 and Figure 8<sup>14</sup>, a summary of the results over the 100 instances is provided.

---

<sup>12</sup>Usually obtained by solving a relaxation of the MILP.

<sup>13</sup>In [43], there is no absolute values (gaps may be negative), no delta (as in Gurobi [28]) and there is no explicit multiplication by 100 to obtain a percentage.

<sup>14</sup>For each figure, the models are sorted in ascending order according to the criterion studied.

Instance	Base models		Improved models						
	$M_1$	$M_2$	$M_3$	$M_4$	$M_5$	$M_6$	$M_7$	$M_8$	$M_9$
#Opt	19	17	53	57	52	55	53	53	50
#Winner	2	1	19	18	13	33	12	18	14
$\overline{R}_i$	8.16	7.82	3.98	3.96	3.86	3.25	4.76	4.33	4.85
$\overline{t}_i$	1.77 h	1.80 h	1.11 h	1.09 h	1.15 h	1.10 h	1.18 h	1.14 h	1.21 h
$\overline{g}_i$	26.66 %	33.90 %	6.42 %	5.27 %	5.89 %	5.13 %	6.91 %	6.81 %	7.35 %

Table 5: Results of the different models: synthesis over the 100 instances.

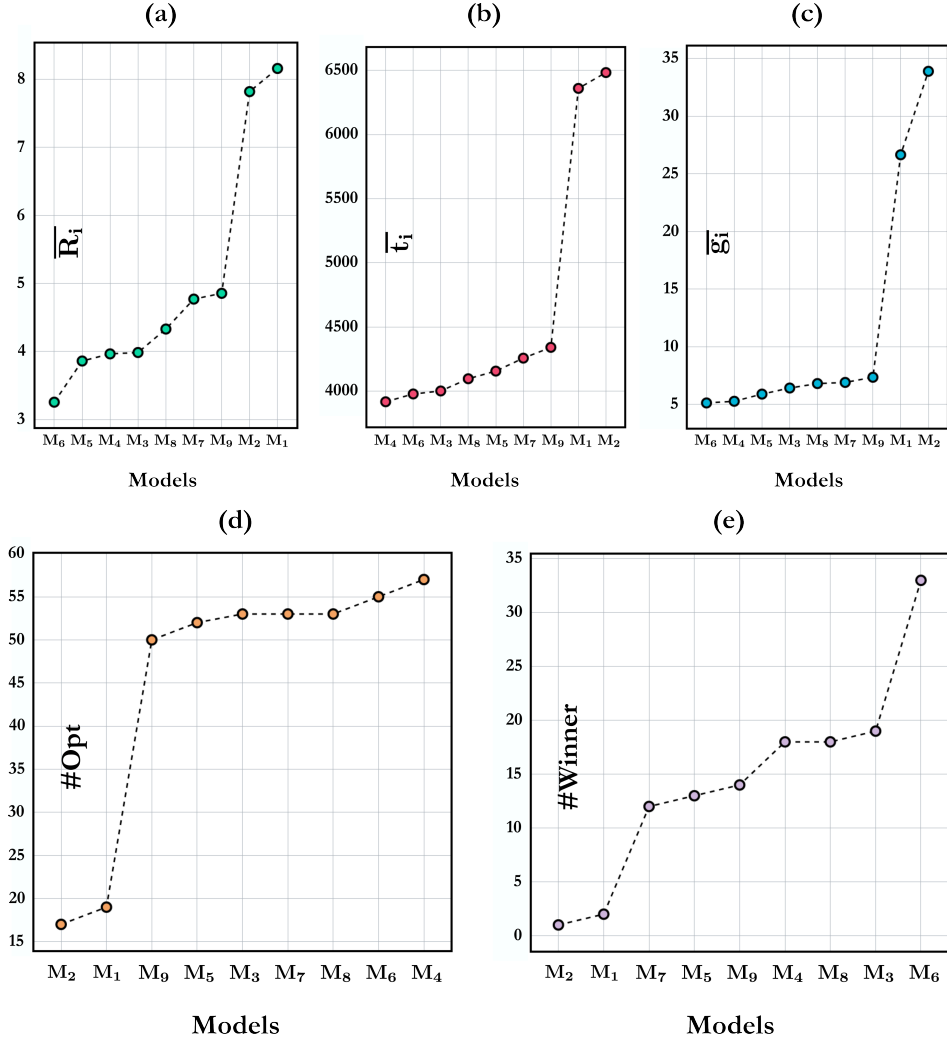


Figure 8: Visualization of results with: average rank (a), average resolution time (b), average relative gap (c), number of instances solved (d) and number of times the formulation performed best (e).

In addition to the above, we provide a set of supplementary appendices, each time with one table per group of 25 instances. First, the full detail of ranks, for each formulation and each instance, are reported in Tables D.14, D.15, D.16 and D.17 in Appendix D. In addition to these ranks, two-by-two comparisons between the different formulations are also available in Tables E.18, E.19, E.20, E.21 in Appendix E. Then, all the integer solutions obtained are reported in Tables C.10, C.11, C.12 and C.13 in Appendix C.

Some examples of solutions are also available in Figure 9. More specifically, there is a focus on one instance for each of the 4 groups, each consisting of 25 instances: peninsula, strait, island and river. For example, for instance no. 36 in the strait group (upper right), we observe a coverage rate of 70.37 % (upper left corner) and the associated optimal solution (network)<sup>15</sup> is made up of

- 1 TxRx buoy of type A (high-frequency) in the center,
- 4 Rx buoys surrounding the TxRx buoy, including:
  - 2 of type F (high-frequency), and,
  - 2 of type E (high-frequency).

Maritime cells are shown in blue and land cells in green. Rhombuses correspond to Tx buoys, circles to Rx buoys and circled rhombuses to TxRx buoys. Finally, the cumulative detection probability is represented by a heatmap with values ranging from 0.1 at the darkest to 1.0 at the lightest.

### 3.3. Statistical Tests (*Non-Parametric*)

In this section, we will analyze the raw results presented above using non-parametric<sup>16</sup> statistical methods in order to conduct a rigorous qualitative analysis. As in [25], we begin with a Friedman test followed by a post-hoc pairwise comparison.

#### 3.3.1. Friedman Test

First, we will use a Friedman test [9, 24] which is based on the ranking of the different formulations on each instance. It is an extension of the sign test when there are more than 2 treatments [9, 16] and the non-parametric analog of one-way repeated-measures ANOVA [45]. To begin with, we will consider the following two hypotheses.

---

<sup>15</sup>Note that the optimal solution systematically uses all available sensors (refer to the GitHub repository mentioned above to find the number of sensors available for each instance).

<sup>16</sup>Making no assumptions about the parameters of the distribution (e.g. variance or mean).

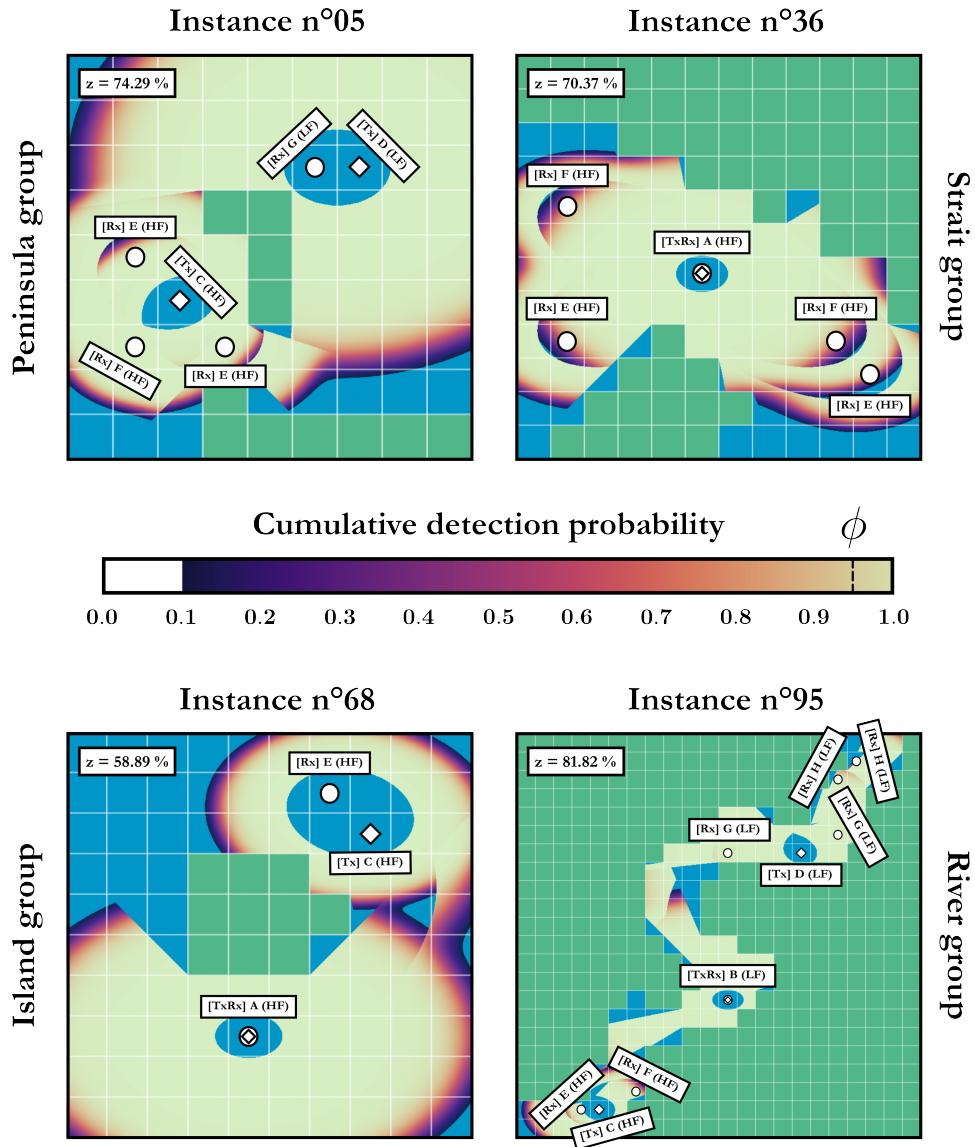


Figure 9: Example of solutions with one instance of each group.

- Null hypothesis  $\mathbf{H}_0$ : for a given instance, all formulations are equally effective or, in other words, each ranking is equally likely (i.e. there is no difference between them).
- Alternative hypothesis  $\mathbf{H}_1$ : at least one formulation tends to be better than at least one other formulation.

The test is subsequently described by

$$T = \begin{cases} \frac{(k-1) \sum_{i=1}^k \left(R_i - \frac{b(k+1)}{2}\right)^2}{A - C} & \text{if there are ties [9] and,} \\ \frac{12}{bk(k+1)} \sum_{i=1}^k \left(R_i - \frac{b(k+1)}{2}\right)^2 & \text{otherwise [24].} \end{cases} \quad (84)$$

In both of these formulas,  $R_i$  is equal to the sum of the ranks of a given formulation  $i \in \llbracket 1, 9 \rrbracket$  over all instances (i.e.  $\sum_{j=1}^k R_{i,j}$ ),  $b$  (block) corresponds to the number of instances (100) and  $k$  (treatments) to the number of formulations (9). Furthermore, for the formula with ties, we have

$$A = \sum_{i=1}^k \sum_{j=1}^b R_{i,j}^2 \text{ and } C = \frac{bk(k+1)^2}{4} \text{ (i.e. the correction factor).}$$

An important assumption is that the variables are mutually independent, which is the case here: the results on one instance (i.e. one block/row) do not influence the results on another instance. As it is difficult to find the exact distribution of  $T$ , an approximation is often used for the null distribution: chi-squared ( $\chi^2$ ) with  $(k-1)$  degrees of freedom [9]. Finally, we have

- $k = 9$ ;  $b = 100$ ;  $A = 28\,265$ ;  $C = 22\,500$ ;  $T = 345.629$ ,
- $\alpha = 0.05$  (significance level) and, lastly,
- $\chi_{\alpha, k-1}^2 = \chi_{0.05, 8}^2 = 15.507$  (critical value).

Thus, with a significant level of  $\alpha = 0.05$ , we can reject the null hypothesis  $\mathbf{H}_0$  ( $T > \chi_{0.05, 8}^2$ ) and conclude that there exist at least one formulation whose performance is different from at least one of the other formulation. In fact, the  $p$ -value associated with the  $T$ -value is about  $7e - 70$  and this means that the null hypothesis could have been rejected at a significance level as low as this.

### 3.3.2. Multiple Comparisons (post-hoc)

The Friedman test having resulted in the rejection of the null hypothesis  $\mathbf{H}_0$ , it is now relevant to perform a post-hoc pairwise comparison of the different formulations. As suggested by Conover in [9], two formulations  $i$  and  $i'$  are considered significantly different if

$$|R_i - R_{i'}| > \underbrace{t_{(1-\frac{\alpha}{2}), (b-1)(k-1)} \cdot \sqrt{\frac{(A-C)2b}{(b-1)(k-1)} \left(1 - \frac{T}{b(k-1)}\right)}}_{\lambda}, \quad (85)$$

where  $R_i$ ,  $A$  and  $C$  are the same as in the previous subsection 3.3.1 and where  $t_{(1-\frac{\alpha}{2}), (b-1)(k-1)}$  is the  $(1 - \frac{\alpha}{2})$  quantile of the Student's t-distribution with  $(b-1)(k-1)$  degrees of freedom (the value for  $\alpha$  is identical to the Friedman test). We therefore have

- $t_{(1-\frac{\alpha}{2}), (b-1)(k-1)} = t_{0.975, 792} = 1.963$  and,
- $\lambda = 56.446$  from equation (85).

Thus, all formulations such that  $|R_i - R_{i'}| > \lambda$  can be considered significantly different with respect to the level of significance  $\alpha = 0.05$ . More precisely,  $M_i$  is said to outperform  $M_{i'}$  at this significant level if  $R_{i'} - R_i > \lambda$  (this implies  $R_i < R_{i'}$ ). A visual representation of the pairwise comparisons may be seen in Figure 10 where the formulations are ordered by sum of the ranks  $R_i$  in ascending order. In addition, the notation  $M_i \succ M_{i'}$  means that formulation  $i$  is significantly better than formulation  $i'$  in the statistical sense and with the significant level  $\alpha = 0.05$ . For each rank  $R_i$ , a vertical segment with length  $\frac{\lambda}{2}$  extends both above and below. In this way, it is possible to visualize when two formulations overlap and two cases can then be distinguished.

- Case 1 (overlap): when there is an overlap (i.e.  $|R_i - R_{i'}| \leq \lambda$ ), then it is not possible to say that one formulation tends to be significantly better than the other.
- Case 2 (no overlap): when there is no overlap (i.e.  $|R_i - R_{i'}| > \lambda$ ), then it is said that the formulation with the lowest rank sum is significantly better than the other.

We first note that the improved models are significantly better than the base models, which also supports the results obtained in [25]. On the other hand, we have formulation  $M_6$  which is significantly better than all other formulations at the significant level  $\alpha = 0.05$ . It is therefore recommended to use this formulation for this problem. Moreover, from Table 5 and Figure 8, we also note that the improved models resolve more than 50 % of the instances while less than 20 % are resolved with the base models. Finally, further experiments could be carried out on a larger dataset with instances (DEMs) of varying dimensions, covering a wider range of different geometric

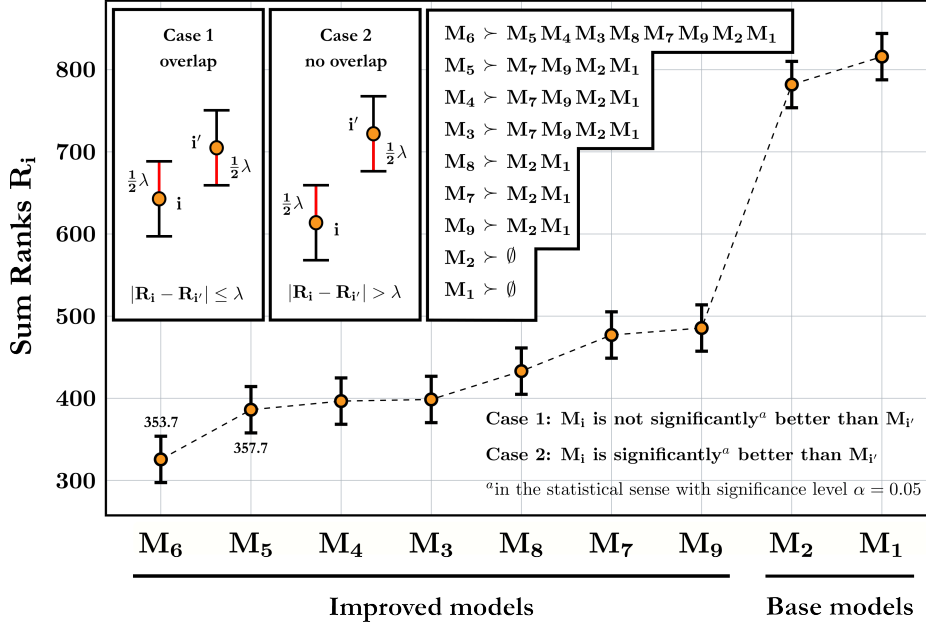


Figure 10: Visual representation of post-hoc pairwise comparisons between the different models.

situations for coastlines. Such a dataset has recently been derived in [56] with 17 700 instances distributed throughout the world’s coastlines and with dimensions ranging from  $10 \times 10$  to  $300 \times 300$  cells.

#### 4. Conclusions and Further Research

In this paper, we addressed the Area Coverage (AC) problem in the scope of optimizing the spatial configuration of heterogeneous multistatic sonar networks with a particular emphasis on acoustic buoys (sonobuoys). The problem of placing buoys that can be transmitter-only (Tx), receiver-only (Rx) and transmitter-receiver (TxRx) as well as of different types with possible incompatibilities and variable performances between source–receiver pairs has, to our knowledge, never been addressed in the literature. In addition, we also take into account some rarely considered aspects such as the direct blast effect, coastlines features and probabilistic detection models, whether taken independently or in combination. For this problem, we have therefore proposed a set of Mixed-Integer Linear Programs (MILPs) to efficiently solve instances of operational interest and we have identified an ideal model, i.e. one that is significantly better than the others in the statistical sense. In particular, this ideal model is an extension of a linearization for quadratic formulations that comes from the literature. Also,



an important point to underline is that the work undertaken here can be easily extended to the dual problem of covering the entire area while trying to minimize the number of buoys used. Moreover, it is also possible to recycle the work undertaken in this study for the AC problem to treat both the Barrier Coverage (BC) and Point Coverage (PC) problems. Indeed, the first one was treated through a reduction to the latter and the BC problem is a special case of AC. Also, it is possible to put greater accent on certain areas by introducing weights on the different targets and to use other detection models, including more realistic ones (e.g. by means of ray-tracing and 2D projection if needed).

Among the perspectives, it would be judicious to try to derive other models based on different linearizations, because the existence of a better model is not to be proscribed. Then, in a perspective of solving more efficiently large-scale instances, it would also be interesting to derive approximate methods such as heuristics or metaheuristics for this newly-defined problem.

## References

- [1] Abbot, P., Dyer, I., 2002. *Sonar Performance Predictions Incorporating Environmental Variability*. Springer Netherlands, Dordrecht. doi:10.1007/978-94-010-0626-2\\_76.
- [2] Ainslie, M., 2010. *Principles of Sonar Performance Modelling*. Springer, Berlin, Heidelberg. doi:10.1007/978-3-540-87662-5.
- [3] Amanatides, J., Woo, A., 1987. A fast voxel traversal algorithm for ray tracing, in: *Proceedings of EuroGraphics*, Amsterdam, Netherlands.
- [4] Been, R., Jaspers, S., Coraluppi, S., Carthel, C., Strode, C., Vermeij, A., 2007. *Multistatic sonar: a road to a maritime network enabled capability*. Technical Report NURC-PR-2007-011.
- [5] Berman, O., Drezner, Z., Krass, D., 2010. Generalized coverage: New developments in covering location models. *Computers & Operations Research* 37, 1675–1687. doi:10.1016/j.cor.2009.11.003.
- [6] Bezanson, J., Edelman, A., Karpinski, S., Shah, V.B., 2017. Julia: A fresh approach to numerical computing. *SIAM review* 59, 65–98. doi:10.1137/141000671.
- [7] Bresenham, J.E., 1965. Algorithm for computer control of a digital plotter. *IBM Systems Journal* 4, 25–30. doi:10.1147/sj.41.0025.
- [8] Chaovalitwongse, W., Pardalos, P.M., Prokopyev, O.A., 2004. A new linearization technique for multi-quadratic 0–1 programming problems. *Operations Research Letters* 32, 517–522. doi:10.1016/j.orl.2004.03.005.
- [9] Conover, W., 1999. *Practical nonparametric statistics*. Wiley series in probability and statistics. 3rd ed., Wiley, New York.

- [10] Coppens, A.B., Sanders, J.V., 1976. An introduction to the sonar equations with applications. Technical Report ADA071133. Naval Postgraduate School. Monterey, California.
- [11] Cox, H., 1989. Fundamentals of Bistatic Active sonar. Springer, Dordrecht. doi:10.1007/978-94-009-2289-1\\_1.
- [12] Craparo, E.M., Fügenschuh, A., Hof, C., Karatas, M., 2019. Optimizing source and receiver placement in multistatic sonar networks to monitor fixed targets. *European Journal of Operational Research* 272, 816–831. doi:10.1016/j.ejor.2018.02.006.
- [13] Craparo, E.M., Karatas, M., 2018. A Method for Placing Sources in Multistatic Sonar Networks. Technical Report NPS-OR-18-001. Naval Postgraduate School. Monterey, California.
- [14] Craparo, E.M., Karatas, M., 2020. Optimal source placement for point coverage in active multistatic sonar networks. *Naval Research Logistics* 67, 63–74. doi:10.1002/nav.21877.
- [15] Craparo, E.M., Karatas, M., Kuhn, T.U., 2017. Sensor placement in active multistatic sonar networks: Active Multistatic Sonar Networks. *Naval Research Logistics* 64, 287–304. doi:10.1002/nav.21746.
- [16] Dixon, W.J., Mood, A.M., 1946. The statistical sign test. *Journal of the American Statistical Association* 41, 557–566.
- [17] Elhabyan, R., Shi, W., St-Hilaire, M., 2019. Coverage protocols for wireless sensor networks: Review and future directions. *Journal of Communications and Networks* 21, 45–60. doi:10.1109/JCN.2019.000005.
- [18] Elminowicz, A., Zajaczkowski, L., 2008. Modeling of underwater sonar barriers. *Journal of the Acoustical Society of America* 123, 3466.
- [19] Elminowicz, A., Zajaczkowski, L., 2006. Multistatic systems. *Hydroacoustics* 9, 57–64.
- [20] Erişkin, L., 2021. Point coverage with heterogeneous sensor networks: A robust optimization approach under target location uncertainty. *Computer Networks* 198, 108416. doi:10.1016/j.comnet.2021.108416.
- [21] Fewell, M., Ozols, S., 2011. Simple detection-performance analysis of multistatic sonar for anti-submarine warfare. Technical Report DSTO-TR-2562. Defence Science and Technology Organisation. Edinburgh, South Australia.
- [22] Fewell, M., Thredgold, J., 2009. Cumulative Track-Initiation Probability as a Basis for Assessing Sonar-System Performance in Anti-Submarine Warfare. Technical Report DSTO-TN-0932. Defence Science and Technology Organisation. Edinburgh, South Australia.
- [23] Fewell, M., Thredgold, J., Kershaw, D., 2008. Benefits of sharing detections for networked track initiation in anti-submarine warfare. Technical Report DSTO-TR-2086. Defence Science and Technology Organisation. Edinburgh, South Australia.
- [24] Friedman, M., 1937. The use of ranks to avoid the assumption of normality implicit in the analysis of variance. *Journal of the American Statistical Association* 32, 675–701. doi:10.1080/01621459.1937.10503522.

- [25] Fügenschuh, A.R., Craparo, E.M., Karatas, M., Buttrey, S.E., 2020. Solving multi-static sonar location problems with mixed-integer programming. *Optimization and Engineering* 21, 273–303. doi:10.1007/s11081-019-09445-2.
- [26] GEBCO Bathymetric Compilation Group, 2022. The GEBCO 2022 grid - a continuous terrain model of the global oceans and land. doi:10.5285/e0f0bb80-ab44-2739-e053-6c86abc0289c.
- [27] Glover, F., 1975. Improved linear integer programming formulations of nonlinear integer problems. *Management Science* 22, 455–460. doi:10.1287/mnsc.22.4.455.
- [28] Gurobi Optimization, LLC, 2023. Gurobi Optimizer Reference Manual. URL: [gurobi.com](http://gurobi.com).
- [29] Guth, P., Niekerk, A., Grohmann, C., Muller, J.P., Hawker, L., Florinsky, I., Gesch, D., Reuter, H., Herrera, V., Riazanoff, S., Lopez-Vazquez, C., Carabajal, C., Albinet, C., Strobl, P., 2021. Digital elevation models: Terminology and definitions. *Remote Sensing* 13, 3581. doi:10.3390/rs13183581.
- [30] Güney, E., Aras, N., Altinel, I.K., Ersoy, C., 2012. Efficient solution techniques for the integrated coverage, sink location and routing problem in wireless sensor networks. *Computers & Operations Research* 39, 1530–1539. doi:10.1016/j.cor.2011.09.002.
- [31] Hervé, C., 2011. Imagerie pour le sonar à ouverture synthétique multistatique (Imaging for multistatic synthetic aperture sonar). Ph.D. thesis. Aix-Marseille 1.
- [32] Hof, C., 2015. Optimization of source and receiver placement in multistatic sonar environments. Master’s thesis. Naval Postgraduate School. Monterey, California. 106 pages.
- [33] Holler, R., Horbach, A., McEachern, J., of Naval Research, U.S.O., 2008. The Ears of Air ASW: A History of U.S. Navy Sonobuoys. Navmar Applied Sciences Corporation, Warminster, Pennsylvania.
- [34] Holler, R.A., 2014. The evolution of the sonobuoy from World War II to the cold war. Technical Report ADA597432. Navmar Applied Sciences Corporation. Warminster, Pennsylvania.
- [35] IBM, 2023. IBM ILOG CPLEX Optimizer. URL: [ibm.com/analytics/cplex-optimizer](http://ibm.com/analytics/cplex-optimizer).
- [36] Iqbal, K., Zhang, M., Piao, S., Ge, H., 2020. Evolution of sonobuoy through history & its applications: A survey, in: 2020 17th International Bhurban Conference on Applied Sciences and Technology (IBCAST), Islamabad, Pakistan. pp. 543–554. doi:10.1109/IBCAST47879.2020.9044549.
- [37] Karatas, M., 2013. A multi foci closed curve: Cassini oval, its properties and applications. *Doğuş Üniversitesi Dergisi* 2, 231–248. doi:10.31671/dogus.2018.108.
- [38] Karatas, M., Craparo, E.M., 2015. Evaluating the direct blast effect in multistatic sonar networks using Monte Carlo simulation, in: 2015 Winter Simulation Conference (WSC), IEEE, Huntington Beach, California, USA. pp. 1184–1194. doi:10.1109/WSC.2015.7408244.
- [39] Karatas, M., Erişkin, L., 2021. The minimal covering location and sizing problem in the presence of gradual cooperative coverage. *European Journal of Operational Research* 295, 838–856. doi:10.1016/j.ejor.2021.03.015.

- [40] Karatas, M., Onggo, B.S., 2019. Optimising the barrier coverage of a wireless sensor network with hub-and-spoke topology using mathematical and simulation models. *Computers & Operations Research* 106, 36–48. doi:10.1016/j.cor.2019.02.007.
- [41] Khoufi, I., Minet, P., Laouiti, A., Mahfoudh, S., 2017. Survey of deployment algorithms in wireless sensor networks: Coverage and connectivity issues and challenges. *International Journal of Autonomous and Adaptive Communications Systems* 10, 341. doi:10.1504/IJAACS.2017.088774.
- [42] Kuhn, T., 2014. Optimal sensor placement in active multistatic sonar networks. Master's thesis. Naval Postgraduate School. Monterey, California. 73 pages.
- [43] Laporte, G., Toth, P., 2022. A gap in scientific reporting. *4OR* 20, 169–171. doi:10.1007/s10288-021-00483-0.
- [44] Lurton, X., 2002. An introduction to underwater acoustics: principles and applications. Springer, London ; New York.
- [45] McCrum-Gardner, E., 2008. Which is the correct statistical test to use? *British Journal of Oral and Maxillofacial Surgery* 46, 38–41.
- [46] McDougall, J., Stoner, E.C., 1938. The computation of Fermi-Dirac functions. *Philosophical Transactions of the Royal Society of London. Series A, Mathematical and Physical Sciences* 237, 67–104. doi:10.1098/rsta.1938.0004.
- [47] Mozzone, L., 1998. Deployable multistatic active sonar: the cycle of system design, tests and data analysis, in: IEEE Oceanic Engineering Society. OCEANS'98. Conference Proceedings (Cat. No.98CH36259), pp. 1547–1552 vol.3. doi:10.1109/OCEANS.1998.726331.
- [48] Ngatchou, P., Fox, W., El-Sharkawi, M., 2006. Multiobjective Multistatic Sonar Sensor Placement, in: 2006 IEEE International Conference on Evolutionary Computation, IEEE, Vancouver, BC, Canada. pp. 2713–2719. doi:10.1109/CEC.2006.1688648.
- [49] Oded Berman, Z.D., Krass, D., 2019. The multiple gradual cover location problem. *Journal of the Operational Research Society* 70, 931–940. doi:10.1080/01605682.2018.1471376.
- [50] Oral, M., Kettani, O., 1992. A Linearization Procedure for Quadratic and Cubic Mixed-Integer Problems. *Operations Research* 40, S109–S116. doi:10.1287/opre.40.1.S109.
- [51] Ozols, S., Fewell, M., 2011. On the design of multistatic sonobuoy fields for area search. Technical Report DSTO-TR-2563. Defence Science and Technology Organisation. Edinburgh, South Australia.
- [52] Raillon, L., Fouquet, M., 2019. Multistatic underwater protection sonar best patterns for harbour and larger critical environments, Stockholm, Sweden. Undersea Defence Technology (UDT).
- [53] Rebai, M., Le berre, M., Snoussi, H., Hnaïen, F., Khoukhi, L., 2015. Sensor deployment optimization methods to achieve both coverage and connectivity in wireless sensor networks. *Computers & Operations Research* 59, 11–21. doi:10.1016/j.cor.2014.11.002.

- [54] Strode, C., Mourre, B., Rixen, M., 2012. Decision support using the Multistatic Tactical Planning Aid (MSTPA). *Ocean Dynamics* 62, 161–175. doi:10.1007/s10236-011-0483-7.
- [55] Swift, M., Riley, J., Lourey, S., Booth, L., 1999. An overview of the multistatic sonar program in australia, in: *ISSPA '99. Proceedings of the Fifth International Symposium on Signal Processing and its Applications (IEEE Cat. No.99EX359)*, Brisbane, QLD, Australia. pp. 321–324 vol.1. doi:10.1109/ISSPA.1999.818177.
- [56] Thuillier, O., Le Josse, N., Olteanu, A.L., Sevaux, M., Tanguy, H., 2024a. Catalogue of coastal-based instances [data set]. doi:10.5281/zenodo.10530247.
- [57] Thuillier, O., Le Josse, N., Olteanu, A.L., Sevaux, M., Tanguy, H., 2024b. An improved two-phase heuristic for active multistatic sonar network configuration. *Expert Systems with Applications* 238, 121985. doi:10.1016/j.eswa.2023.121985.
- [58] Tollefsen, C.D., 2016. Multistatic Planning Requirements. Technical Report DRDC-RDDC-2016-R090. Defence Research and Development Canada (DRDC). Atlantic Research Centre.
- [59] Urick, R.J., 1983. *Principles of underwater sound*. 3rd ed., McGraw-Hill, New York.
- [60] Washburn, A.R., 2010. A multistatic sonobuoy theory. Technical Report NPS-OR-10-005. Naval Postgraduate School. Monterey, California.
- [61] Washburn, A.R., Karatas, M., 2015. Multistatic search theory. *Military Operations Research* 20, 21–38. doi:10.5711/1082598320121.
- [62] Ziling, Z., Erzhang, F., Xuanzi, Y., Chenyang, G., 2021. Detection performance analysis of multistatic sonar system based on cumulative detection, in: *2021 OES China Ocean Acoustics (COA)*, pp. 601–608. doi:10.1109/COA50123.2021.9520022.

## Appendix A. Direct Blast Effect: Mathematical Details

In this appendix, we will give the mathematical details of equation 19, starting with the monostatic case and ending with the bistatic case, which is more general. Both cases are illustrated in Figure A.11.

### Appendix A.1. Monostatic case

First of all, for a sonar system in monostatic configuration, suppose that the source emits a sound pulse (ping) in the time interval  $[0, \tau]$  (emission of  $\tau$  seconds) and that a target is at a distance  $d = d_{s,t} = d_{t,r}$ , in km, from this sonar system. Thus, the signal reflected by the target (the echo) will arrive at the receiver (collocated with the source) in the time interval  $[\frac{2d}{c}, \frac{2d}{c} + \tau]$  where the first term corresponds to the starting time of reception of the signal and the second term to the ending time of reception of the signal. Finally, detection will not be possible if the receiver starts to receive the reflected signal while the source is still transmitting<sup>17</sup>, or, in other words, if

$$\frac{2d}{c} < \tau \Leftrightarrow d < \frac{c\tau}{2}, \quad (\text{A.1})$$

with  $r_b = \frac{c\tau}{2}$  equal to half the pulse length. In terms of geometric interpretation, this gives us a circle of radius  $r_b$  centered on the sonar system and within which detection is theoretically impossible.

### Appendix A.2. Bistatic case

For a sonar system in bistatic configuration, the signal from the direct path<sup>18</sup> will arrive at the receiver in the time interval  $[\frac{d_{s,r}}{c}, \frac{d_{s,r}}{c} + \tau]$  while the signal reflected by the target will arrive at the receiver in the time interval  $[\frac{d_{s,t}+d_{t,r}}{c}, \frac{d_{s,t}+d_{t,r}}{c} + \tau]$ . Indeed, there is the source-target path and the target-receiver path to take into account for the reflected signal. Finally, detection will not be possible if the receiver starts to receive the reflected signal while it is still receiving the signal from the direct path, or, in other words, if

$$\frac{d_{s,t} + d_{t,r}}{c} < \frac{d_{s,r}}{c} + \tau, \quad (\text{A.2})$$

$$\Leftrightarrow d_{s,t} + d_{t,r} < d_{s,r} + c\tau, \quad [\times c] \quad (\text{A.3})$$

$$\Leftrightarrow d_{s,t} + d_{t,r} < d_{s,r} + 2r_b. \quad \left[ r_b = \frac{c\tau}{2} \Leftrightarrow c\tau = 2r_b \right] \quad (\text{A.4})$$

---

<sup>17</sup>This implies that the receiver receives both the signal from the initial pulse and the reflected signal.

<sup>18</sup>The direct path corresponds to the signal received directly from the source, without reflection.

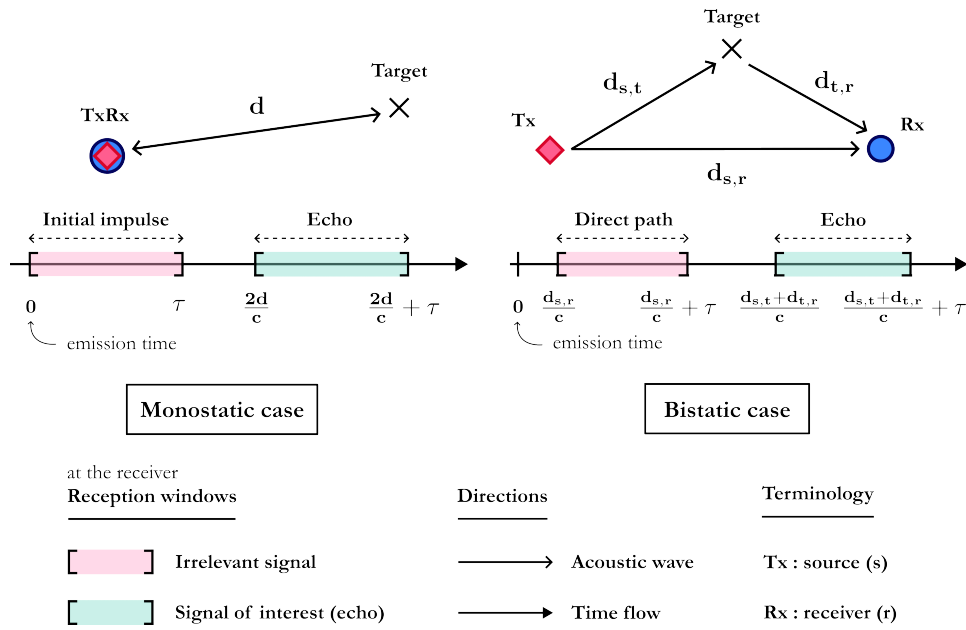


Figure A.11: Illustration of the direct blast effect.

In terms of geometric interpretation, we find here the masking ellipse mentioned in the paper, the foci of which are respectively the source and the receiver (non-colocated).

## Appendix B. Raw Results

### Appendix B.1. Group 1: Peninsula

Instance	Base models		Improved models						
	$M_1$	$M_2$	$M_3$	$M_4$	$M_5$	$M_6$	$M_7$	$M_8$	$M_9$
01	174.05	875.77	29.39	<b>28.76</b>	29.83	29.70	30.16	30.17	31.45
02	964.80	437.96	21.28	20.68	23.58	23.20	23.29	<b>18.21</b>	22.67
03	6272.77	4777.70	21.30	21.55	23.08	20.80	<b>19.96</b>	20.53	32.94
04	125.81 %	125.81 %	2903.74	2939.29	<b>1662.68</b>	1697.41	1713.28	1693.97	2134.67
05	40.00 %	37.25 %	21.83 %	<b>1085.14</b>	8.88 %	5330.95	5887.73	30.94 %	5611.91
06	25.00 %	20.69 %	8.33 %	<b>6.95 %</b>	7.58 %	13.46 %	11.65 %	16.20 %	15.19 %
07	4096.32	3413.19	1778.53	2727.83	1686.15	<b>1027.63</b>	4564.15	2675.17	4445.71
08	42.86 %	42.86 %	<b>3295.51</b>	5467.09	6.79 %	14.80 %	27.05 %	23.69 %	9.43 %
09	4.48 %	2.94 %	3050.74	<b>1417.95</b>	2091.30	1611.94	2627.39	2598.94	2443.21
10	2171.50	438.44	31.66	46.48	<b>23.60</b>	33.94	41.68	64.38	65.37
11	29.63 %	25.00 %	<b>8.50 %</b>	14.35 %	12.50 %	9.06 %	12.59 %	8.93 %	12.52 %
12	866.86	150.39	39.30	157.30	23.04	<b>19.96</b>	44.08	56.91	70.51
13	11.11 %	11.11 %	7.79 %	6.06 %	<b>5.23 %</b>	9.37 %	7.39 %	7.69 %	7.61 %
14	7.69 %	7.69 %	<b>782.38</b>	1834.73	1551.69	1044.09	2641.57	7142.94	5397.93
15	1.45 %	1.45 %	<b>158.25</b>	1.45 %	312.87	359.90	1017.04	1012.46	5493.56
16	94.44 %	94.44 %	1376.17	1350.04	5373.24	5531.39	5210.17	<b>1150.11</b>	2916.12
17	7.69 %	9.37 %	6849.61	6679.77	4094.51	1.52 %	<b>3266.10</b>	3588.69	3.03 %
18	4.48 %	6.06 %	2.94 %	4.48 %	2.94 %	2.94 %	<b>7049.85</b>	2.94 %	2.94 %
19	12.90 %	11.11 %	6.21 %	7.81 %	<b>5.46 %</b>	7.80 %	12.90 %	11.03 %	9.23 %
20	48.94 %	52.17 %	48.55 %	48.43 %	21.63 %	<b>21.61 %</b>	27.06 %	45.01 %	31.30 %
21	4506.07	2236.99	1032.72	760.22	724.38	<b>311.66</b>	1385.66	3255.87	450.90
22	4852.25	538.43	190.81	192.13	92.28	48.78	<b>42.38</b>	212.64	76.91
23	1314.93	3140.98	<b>27.65</b>	71.13	34.12	35.86	36.52	36.66	114.15
24	1.45 %	1.45 %	74.93	332.23	397.20	<b>66.05</b>	147.57	98.63	1103.48
25	2.94 %	2.94 %	446.30	287.93	403.17	239.18	288.64	<b>167.70</b>	715.99
#Opt / 25	9	9	18	18	17	17	19	17	17
#Winner	0	0	5	4	4	5	4	3	0
$\overline{R}_i$	8.50	8.14	3.56	4.26	3.28	3.12	4.42	4.44	5.28
$\overline{t}_i$	1.56 h	1.46 h	0.81 h	0.84 h	0.85 h	0.83 h	0.88 h	0.90 h	0.99 h
$\overline{g}_i$	18.43 %	18.09 %	4.17 %	3.58 %	2.84 %	3.22 %	3.95 %	5.86 %	3.65 %

Table B.6: Results of the different formulations: CPU time (s) or relative gap if computational budget is reached.  $\overline{R}_i$  (resp.  $\overline{t}_i$ ,  $\overline{g}_i$ ) is the average rank (resp. average CPU time, average relative gap) of model  $i \in \llbracket 1, 9 \rrbracket$ . **Peninsula instance group:  $9 \times 9$  grid with 70 maritime cells (1/4).**



Appendix B.2. Group 2: Detroit


 Instance	Base models		Improved models						
	$M_1$	$M_2$	$M_3$	$M_4$	$M_5$	$M_6$	$M_7$	$M_8$	$M_9$
26	1.25 %	1.25 %	59.99	251.59	77.39	<b>57.06</b>	705.02	673.46	803.67
27	8.00 %	9.46 %	6.67 %	6.67 %	6.67 %	<b>4.33 %</b>	8.11 %	6.67 %	6.67 %
28	5.19 %	2.53 %	2.51 %	2.53 %	2.53 %	<b>1.27 %</b>	2.53 %	<b>1.27 %</b>	2.53 %
29	3726.91	334.15 %	<b>233.80</b>	242.55	746.60	767.20	785.12	812.15	265.41
30	159.14 %	216.67 %	1368.70	1498.22	2454.23	2391.81	2574.78	1537.79	<b>87.53</b>
31	5484.48	161.84 %	1088.96	<b>996.66</b>	2854.12	3025.97	2929.29	3015.78	4055.86
32	28.57 %	22.73 %	31.15 %	<b>16.18 %</b>	19.40 %	20.78 %	20.90 %	19.40 %	17.65 %
33	30.65 %	19.12 %	<b>8.32 %</b>	11.11 %	12.86 %	12.68 %	17.39 %	14.08 %	17.39 %
34	24.62 %	10.96 %	12.68 %	9.48 %	8.11 %	<b>4.05 %</b>	9.46 %	14.07 %	10.56 %
35	8.00 %	8.00 %	<b>5.19 %</b>	6.58 %	<b>5.19 %</b>	<b>5.19 %</b>	8.00 %	6.58 %	<b>5.19 %</b>
36	5667.39	40.94 %	1623.94	<b>1518.76</b>	1641.42	1641.12	2471.52	2865.34	6669.40
37	10.96 %	9.46 %	7.93 %	9.53 %	9.59 %	<b>6058.52</b>	9.59 %	10.95 %	9.34 %
38	3994.32	2197.19	441.53	1014.09	523.58	1119.19	2295.08	<b>282.13</b>	1.25 %
39	20.90 %	12.50 %	12.66 %	15.94 %	9.59 %	<b>9.55 %</b>	9.59 %	11.11 %	12.50 %
40	5.19 %	5.19 %	3.90 %	4138.34	3884.00	2.54 %	3308.58	<b>2433.49</b>	1.27 %
41	1.25 %	2.53 %	25.00 %	506.18	507.89	<b>384.97</b>	4832.98	1809.47	1162.20
42	26.56 %	26.56 %	26.56 %	26.56 %	<b>24.62 %</b>	26.56 %	26.56 %	37.29 %	32.79 %
43	26.56 %	20.90 %	<b>19.12 %</b>	20.90 %	20.90 %	30.65 %	28.57 %	22.73 %	32.79 %
44	24.62 %	28.57 %	24.62 %	19.12 %	22.73 %	<b>17.39 %</b>	24.62 %	19.12 %	19.12 %
45	<b>2.53 %</b>	3.85 %	<b>2.53 %</b>	3.85 %	3.85 %	5.19 %	3.85 %	3.85 %	<b>2.53 %</b>
46	5.19 %	<b>1.25 %</b>	2.53 %	2.53 %	2.53 %	<b>1.25 %</b>	<b>1.25 %</b>	2.53 %	2.53 %
47	<b>3.90 %</b>	5.19 %	5.19 %	5.19 %	5.19 %	5.19 %	5.19 %	5.19 %	5.19 %
48	5.19 %	3.85 %	3.81 %	3.85 %	3.85 %	<b>2.56 %</b>	<b>2.56 %</b>	3.85 %	<b>2.56 %</b>
49	17.39 %	20.90 %	17.39 %	17.39 %	<b>14.08 %</b>	22.73 %	19.12 %	<b>14.08 %</b>	19.12 %
50	37.29 %	39.66 %	28.57 %	24.62 %	<b>22.73 %</b>	<b>22.73 %</b>	<b>22.73 %</b>	<b>22.73 %</b>	26.56 %
#Opt / 25	4	1	6	8	8	8	8	8	6
#Winner	2	1	5	3	4	12	3	5	4
$\overline{R}_i$	7.26	6.96	4.13	4.00	3.88	3.66	5.30	4.74	5.05
$\overline{t}_i$	1.89 h	1.94 h	1.57 h	1.47 h	1.50 h	1.53 h	1.58 h	1.51 h	1.66 h
$\overline{g}_i$	18.12 %	40.32 %	9.85 %	8.08 %	7.78 %	7.79 %	8.80 %	8.62 %	9.10 %

Table B.7: Results of the different formulations: CPU time (s) or relative gap if computational budget is reached.  $\overline{R}_i$  (resp.  $\overline{t}_i$ ,  $\overline{g}_i$ ) is the average rank (resp. average CPU time, average relative gap) of model  $i \in \llbracket 1, 9 \rrbracket$ . **Strait instance group:  $12 \times 12$  grid with 81 maritime cells (2/4).**

Appendix B.3. Group 3: Island


 Instance	Base models		Improved models						
	$M_1$	$M_2$	$M_3$	$M_4$	$M_5$	$M_6$	$M_7$	$M_8$	$M_9$
51	1273.73	260.54 %	80.50	77.47	80.92	79.72	82.81	78.70	<b>71.03</b>
52	227.07	92.00 %	<b>48.72</b>	51.59	49.87	50.04	52.20	50.40	60.27
53	210.34 %	200.00 %	186.30	186.43	45.61	46.21	43.89	<b>41.31</b>	189.80
54	119.51 %	119.51 %	10.91 %	<b>10.60 %</b>	25.58 %	24.56 %	24.85 %	24.60 %	74.72 %
55	28.57 %	23.29 %	20.00 %	28.57 %	18.42 %	<b>16.88 %</b>	20.00 %	18.42 %	32.35 %
56	9.76 %	2.27 %	<b>1.12 %</b>	<b>1.12 %</b>	2.27 %	<b>1.12 %</b>	<b>1.12 %</b>	<b>1.12 %</b>	3.45 %
57	3557.42	1.12 %	<b>105.28</b>	2817.11	1524.21	1377.47	401.20	1358.52	816.02
58	18.42 %	18.42 %	9.76 %	18.42 %	9.76 %	<b>8.43 %</b>	12.50 %	11.11 %	15.38 %
59	23.29 %	26.76 %	8.43 %	<b>7.14 %</b>	8.43 %	<b>7.14 %</b>	12.50 %	<b>7.14 %</b>	<b>7.14 %</b>
60	5.88 %	7.14 %	4.65 %	<b>2.27 %</b>	3.45 %	3.45 %	8.43 %	<b>2.27 %</b>	3.45 %
61	18.42 %	8.43 %	5.88 %	<b>4.65 %</b>	<b>4.65 %</b>	5.88 %	<b>4.65 %</b>	5.88 %	5.88 %
62	15.38 %	4.65 %	2.27 %	2.27 %	2.27 %	<b>1.12 %</b>	<b>1.12 %</b>	2.27 %	3.45 %
63	1.12 %	1.12 %	1258.26	1.12 %	1.12 %	1661.96	1.12 %	<b>530.70</b>	3850.00
64	45.16 %	28.57 %	<b>25.22 %</b>	27.90 %	25.71 %	25.61 %	25.71 %	28.57 %	28.57 %
65	15.38 %	18.42 %	13.00 %	12.66 %	13.50 %	10.00 %	13.44 %	12.66 %	<b>9.95 %</b>
66	8.43 %	7.14 %	7.32 %	13.55 %	4.76 %	4.76 %	4.76 %	8.43 %	<b>3.53 %</b>
67	4.65 %	1.12 %	1.12 %	<b>2197.81</b>	1.12 %	1.12 %	1.12 %	2.27 %	2.27 %
68	69.81 %	69.81 %	56.36 %	4973.01	60.01 %	<b>3763.32</b>	64.76 %	50.75 %	67.03 %
69	4.65 %	5015.11	<b>685.44</b>	1227.08	1557.24	1151.78	2575.88	3191.72	985.65
70	2.27 %	2.27 %	2059.04	1782.85	<b>418.79</b>	2191.69	1815.41	953.10	539.63
71	12.50 %	7.14 %	4.64 %	6960.56	8.63 %	<b>4268.47</b>	5673.47	9.65 %	9.87 %
72	2.27 %	2.27 %	3251.40	2518.65	<b>927.68</b>	2323.24	1024.93	1.12 %	4816.57
73	2.27 %	2.27 %	260.70	677.59	390.53	745.25	477.57	222.94	<b>146.28</b>
74	2.27 %	5217.51	1142.05	148.65	443.90	<b>101.53</b>	163.16	167.45	917.32
75	2.27 %	6293.62	384.82	895.84	117.65	<b>67.47</b>	155.80	119.79	229.79
#Opt / 25	3	3	11	13	10	13	11	10	11
#Winner	0	0	5	6	3	9	3	5	5
$\overline{R}_i$	8.38	7.68	3.98	4.30	4.16	3.02	4.42	4.08	4.98
$\overline{t}_i$	1.82 h	1.94 h	1.23 h	1.23 h	1.26 h	1.16 h	1.26 h	1.27 h	1.26 h
$\overline{g}_i$	24.90 %	36.17 %	6.83 %	5.21 %	7.59 %	4.40 %	7.84 %	7.45 %	10.68 %

Table B.8: Results of the different formulations: CPU time (s) or relative gap if computational budget is reached.  $\overline{R}_i$  (resp.  $\overline{t}_i$ ,  $\overline{g}_i$ ) is the average rank (resp. average CPU time, average relative gap) of model  $i \in \llbracket 1, 9 \rrbracket$ . **Island instance group:  $10 \times 10$  grid with 90 maritime cells (3/4).**

Appendix B.4. Group 4: River


 Instance	Base models		Improved models						
	$M_1$	$M_2$	$M_3$	$M_4$	$M_5$	$M_6$	$M_7$	$M_8$	$M_9$
76	1250.53	1828.11	26.20	21.96	22.41	<b>19.86</b>	21.27	22.46	24.56
77	1512.51	6215.72	18.04	16.67	17.01	<b>15.66</b>	16.68	17.12	19.53
78	211.19 %	241.38 %	486.69	479.20	491.71	460.51	475.53	937.75	<b>435.14</b>
79	98.00 %	98.00 %	40.70 %	<b>33.76 %</b>	54.37 %	50.19 %	54.96 %	46.81 %	43.35 %
80	130.23 %	125.00 %	703.08	<b>583.10</b>	7.94 %	7.18 %	19.64 %	3192.05	24.15 %
81	115.22 %	125.00 %	<b>1956.40</b>	2104.54	3314.67	3326.70	11.85 %	6175.95	4.00 %
82	52.31 %	52.31 %	<b>15.67 %</b>	16.66 %	17.77 %	19.76 %	25.05 %	28.94 %	16.10 %
83	19.28 %	11.24 %	5.00 %	3.03 %	<b>2.18 %</b>	3.28 %	7.62 %	5.33 %	2.52 %
84	20.73 %	12.50 %	8.61 %	6.29 %	7.95 %	<b>4.22 %</b>	9.40 %	9.24 %	6.50 %
85	10.00 %	15.12 %	6.01 %	6.67 %	4.38 %	5.02 %	6.93 %	5.73 %	<b>3.70 %</b>
86	8.79 %	4.21 %	4196.69	2861.85	6346.37	<b>2057.99</b>	1.03 %	5227.73	3417.48
87	3.12 %	2.06 %	729.05	1197.42	<b>175.13</b>	432.02	362.63	1410.73	999.48
88	2.06 %	2.06 %	4484.81	3072.78	2463.16	2705.88	<b>1635.97</b>	3507.04	3326.87
89	4.21 %	7.61 %	<b>1.02 %</b>	<b>1.02 %</b>	2.06 %	<b>1.02 %</b>	<b>1.02 %</b>	<b>1.02 %</b>	<b>1.02 %</b>
90	3.12 %	1.02 %	1324.37	588.90	585.56	<b>40.73</b>	735.90	586.47	405.63
91	824.95	4108.96	77.30	<b>52.40</b>	102.14	174.40	389.83	357.97	408.71
92	81.48 %	81.61 %	295.85	<b>121.78</b>	251.36	466.62	2939.29	454.45	835.15
93	129.91 %	3800.73	18.67	16.70	20.24	18.20	20.23	17.16	<b>14.73</b>
94	73.68 %	83.33 %	4694.43	3265.83	3754.60	4116.41	650.91	1521.90	<b>544.04</b>
95	35.62 %	30.26 %	2043.78	2210.33	6820.38	5962.93	2489.58	<b>1677.60</b>	2617.82
96	23.75 %	33.78 %	<b>98.39</b>	423.26	673.36	1265.16	2794.23	482.38	885.56
97	15.12 %	8.79 %	1534.63	2687.39	7132.49	<b>1078.18</b>	5299.81	1161.28	1599.12
98	7.61 %	4.21 %	2107.21	1663.89	694.90	600.12	787.99	<b>255.38</b>	1282.52
99	50.00 %	57.14 %	43.92 %	37.85 %	37.59 %	36.67 %	38.44 %	<b>35.53 %</b>	48.16 %
100	33.78 %	28.57 %	517.91	603.39	324.03	320.07	260.89	<b>257.67</b>	482.96
#Opt / 25	3	4	18	18	17	17	15	18	16
#Winner	0	0	4	5	2	7	2	5	5
$\overline{R}_i$	8.50	8.50	4.26	3.30	4.12	3.22	4.94	4.05	4.09
$\overline{t}_i$	1.80 h	1.86 h	0.84 h	0.80 h	1.01 h	0.90 h	1.01 h	0.86 h	0.91 h
$\overline{g}_i$	45.17 %	41.01 %	4.84 %	4.21 %	5.37 %	5.09 %	7.04 %	5.30 %	5.98 %

Table B.9: Results of the different formulations: CPU time (s) or relative gap if computational budget is reached.  $\overline{R}_i$  (resp.  $\overline{t}_i$ ,  $\overline{g}_i$ ) is the average rank (resp. average CPU time, average relative gap) of model  $i \in \llbracket 1, 9 \rrbracket$ . **River instance group:  $22 \times 22$  grid with 99 maritime cells (4/4).**

## Appendix C. Solutions

### Appendix C.1. Group 1: Peninsula

Instance	Base		Group 1							$z^{Best}$
	$M_1$	$M_2$	$M_3$	$M_4$	$M_5$	$M_6$	$M_7$	$M_8$	$M_9$	
01	22.86	22.86	22.86	22.86	22.86	22.86	22.86	22.86	22.86	22.86*
02	30.00	30.00	30.00	30.00	30.00	30.00	30.00	30.00	30.00	30.00*
03	31.43	31.43	31.43	31.43	31.43	31.43	31.43	31.43	31.43	31.43*
04	44.29	44.29	45.71	45.71	45.71	45.71	45.71	45.71	45.71	45.71*
05	71.43	72.86	74.29	74.29	72.86	74.29	74.29	72.86	74.29	74.29*
06	80.00	82.86	85.71	85.71	85.71	84.29	85.71	84.29	84.29	85.71
07	90.00	90.00	90.00	90.00	90.00	90.00	90.00	90.00	90.00	90.00*
08	70.00	70.00	72.86	72.86	72.86	72.86	72.86	72.86	72.86	72.86*
09	95.71	97.14	98.57	98.57	98.57	98.57	98.57	98.57	98.57	98.57*
10	97.14	97.14	97.14	97.14	97.14	97.14	97.14	97.14	97.14	97.14*
11	77.14	80.00	80.00	78.57	80.00	80.00	80.00	80.00	80.00	80.00
12	97.14	97.14	97.14	97.14	97.14	97.14	97.14	97.14	97.14	97.14*
13	90.00	90.00	91.43	92.86	92.86	91.43	92.86	92.86	92.86	92.86
14	92.86	92.86	92.86	92.86	92.86	92.86	92.86	92.86	92.86	92.86*
15	98.57	98.57	98.57	98.57	98.57	98.57	98.57	98.57	98.57	98.57*
16	51.43	51.43	52.86	52.86	52.86	52.86	52.86	52.86	52.86	52.86*
17	92.86	91.43	94.29	94.29	94.29	94.29	94.29	94.29	94.29	94.29*
18	95.71	94.29	97.14	95.71	97.14	97.14	98.57	97.14	97.14	98.57*
19	88.57	90.00	91.43	91.43	91.43	91.43	88.57	90.00	91.43	91.43
20	67.14	65.71	65.71	65.71	67.14	67.14	67.14	67.14	67.14	67.14
21	92.86	92.86	92.86	92.86	92.86	92.86	92.86	92.86	92.86	92.86*
22	97.14	97.14	97.14	97.14	97.14	95.71	97.14	97.14	97.14	97.14*
23	97.14	97.14	97.14	97.14	97.14	97.14	97.14	97.14	97.14	97.14*
24	98.57	98.57	100.00	100.00	100.00	100.00	100.00	100.00	100.00	100.00*
25	97.14	97.14	97.14	97.14	97.14	97.14	97.14	97.14	97.14	97.14*

Table C.10: Coverage rate (in %) associated with the best integer solutions for each of the formulations. The grey background means that the instance has not been resolved.  $z^{Best}$  is the coverage rate (in %) of the best known integer solution for the considered instance and the presence of an asterisk means that it is the optimal solution. Peninsula instance group (1/4).

Appendix C.2. Group 2: Detroit

Instance	Base		Group 1							$z^{Best}$
	$M_1$	$M_2$	$M_3$	$M_4$	$M_5$	$M_6$	$M_7$	$M_8$	$M_9$	
26	98.77	98.77	98.77	98.77	98.77	98.77	98.77	98.77	98.77	98.77*
27	92.59	91.36	92.59	92.59	92.59	92.59	91.36	92.59	92.59	92.59
28	95.06	97.53	97.53	97.53	97.53	97.53	97.53	97.53	97.53	97.53
29	20.99	20.99	20.99	20.99	20.99	20.99	20.99	20.99	20.99	20.99*
30	32.10	29.63	32.10	32.10	32.10	32.10	32.10	32.10	32.10	32.10*
31	34.57	34.57	34.57	34.57	34.57	34.57	34.57	34.57	34.57	34.57*
32	77.78	81.48	75.31	83.95	82.72	82.72	82.72	82.72	83.95	83.95
33	76.54	83.95	88.89	88.89	86.42	87.65	85.19	87.65	85.19	88.89
34	80.25	90.12	87.65	90.12	91.36	91.36	91.36	87.65	90.12	91.36
35	92.59	92.59	95.06	93.83	95.06	95.06	92.59	93.83	95.06	95.06
36	70.37	70.37	70.37	70.37	70.37	70.37	70.37	70.37	70.37	70.37*
37	90.12	91.36	91.36	90.12	90.12	91.36	90.12	90.12	91.36	91.36*
38	100.00	100.00	100.00	100.00	100.00	100.00	100.00	100.00	98.77	100.00*
39	82.72	88.89	87.65	85.19	90.12	90.12	90.12	88.89	88.89	90.12
40	95.06	95.06	95.06	97.53	97.53	96.30	97.53	97.53	97.53	97.53*
41	98.77	97.53	79.01	98.77	98.77	98.77	98.77	98.77	98.77	98.77*
42	79.01	79.01	79.01	79.01	80.25	79.01	79.01	72.84	75.31	80.25
43	79.01	82.72	83.95	82.72	82.72	76.54	77.78	81.48	75.31	83.95
44	80.25	77.78	80.25	83.95	81.48	85.19	80.25	83.95	83.95	85.19
45	97.53	96.30	97.53	96.30	96.30	95.06	96.30	96.30	97.53	97.53
46	95.06	98.77	97.53	97.53	97.53	98.77	98.77	97.53	97.53	98.77
47	95.06	95.06	95.06	95.06	95.06	95.06	95.06	95.06	95.06	95.06
48	95.06	96.30	96.30	96.30	96.30	96.30	96.30	96.30	96.30	96.30
49	85.19	82.72	85.19	85.19	87.65	81.48	83.95	87.65	83.95	87.65
50	72.84	71.60	77.78	80.25	81.48	81.48	81.48	81.48	79.01	81.48

Table C.11: Coverage rate (in %) associated with the best integer solutions for each of the formulations. The grey background means that the instance has not been resolved.  $z^{Best}$  is the coverage rate (in %) of the best known integer solution for the considered instance and the presence of an asterisk means that it is the optimal solution. Detroit instance group (2/4).

Appendix C.3. Group 3: Island

Instance	Base		Group 1							$z^{Best}$
	$M_1$	$M_2$	$M_3$	$M_4$	$M_5$	$M_6$	$M_7$	$M_8$	$M_9$	
51	23.33	23.33	23.33	23.33	23.33	23.33	23.33	23.33	23.33	23.33*
52	27.78	27.78	27.78	27.78	27.78	27.78	27.78	27.78	27.78	27.78*
53	32.22	33.33	33.33	33.33	33.33	33.33	33.33	33.33	33.33	33.33*
54	45.56	45.56	45.56	45.56	45.56	45.56	45.56	45.56	45.56	45.56
55	77.78	81.11	83.33	77.78	84.44	85.56	83.33	84.44	75.56	85.56
56	91.11	97.78	98.89	98.89	97.78	98.89	98.89	98.89	96.67	98.89
57	100.00	98.89	100.00	100.00	100.00	100.00	100.00	100.00	100.00	100.00*
58	84.44	84.44	91.11	84.44	91.11	92.22	88.89	90.00	86.67	92.22
59	81.11	78.89	92.22	93.33	92.22	93.33	88.89	93.33	93.33	93.33
60	94.44	93.33	95.56	97.78	96.67	96.67	92.22	97.78	96.67	97.78
61	84.44	92.22	94.44	95.56	95.56	94.44	95.56	94.44	94.44	95.56
62	86.67	95.56	97.78	97.78	97.78	98.89	98.89	97.78	96.67	98.89
63	98.89	98.89	100.00	98.89	98.89	100.00	98.89	100.00	100.00	100.00*
64	68.89	77.78	77.78	75.56	77.78	77.78	77.78	77.78	77.78	77.78
65	86.67	84.44	86.67	87.78	87.78	88.89	86.67	87.78	88.89	88.89
66	92.22	93.33	91.11	86.67	93.33	93.33	93.33	92.22	94.44	94.44
67	95.56	98.89	98.89	98.89	98.89	98.89	98.89	97.78	97.78	98.89*
68	58.89	58.89	57.78	58.89	58.89	58.89	57.78	58.89	57.78	58.89*
69	95.56	95.56	95.56	95.56	95.56	95.56	95.56	95.56	95.56	95.56*
70	97.78	97.78	97.78	97.78	97.78	97.78	97.78	97.78	97.78	97.78*
71	88.89	93.33	93.33	93.33	90.00	93.33	93.33	88.89	90.00	93.33*
72	97.78	97.78	98.89	98.89	98.89	98.89	98.89	98.89	98.89	98.89*
73	97.78	97.78	97.78	97.78	97.78	97.78	97.78	97.78	97.78	97.78*
74	97.78	97.78	97.78	97.78	97.78	97.78	97.78	97.78	97.78	97.78*
75	97.78	97.78	97.78	97.78	97.78	97.78	97.78	97.78	97.78	97.78*

Table C.12: Coverage rate (in %) associated with the best integer solutions for each of the formulations. The grey background means that the instance has not been resolved.  $z^{Best}$  is the coverage rate (in %) of the best known integer solution for the considered instance and the presence of an asterisk means that it is the optimal solution. Island instance group (3/4).

Appendix C.4. Group 4: River

Instance	Base		Group 1							$z^{Best}$
	$M_1$	$M_2$	$M_3$	$M_4$	$M_5$	$M_6$	$M_7$	$M_8$	$M_9$	
76	17.17	17.17	17.17	17.17	17.17	17.17	17.17	17.17	17.17	17.17*
77	20.20	20.20	20.20	20.20	20.20	20.20	20.20	20.20	20.20	20.20*
78	31.31	29.29	32.32	32.32	32.32	32.32	32.32	32.32	32.32	32.32*
79	50.51	50.51	51.52	52.53	51.52	52.53	52.53	52.53	51.52	52.53
80	43.43	44.44	45.45	45.45	45.45	44.44	44.44	45.45	44.44	45.45*
81	46.46	44.44	50.51	50.51	50.51	50.51	49.49	50.51	50.51	50.51*
82	65.66	65.66	67.68	68.69	67.68	67.68	66.67	64.65	69.70	69.70
83	83.84	89.90	90.91	91.92	91.92	91.92	89.90	90.91	91.92	91.92
84	82.83	88.89	88.89	90.91	88.89	90.91	87.88	88.89	89.90	90.91
85	90.91	86.87	90.91	90.91	91.92	91.92	89.90	90.91	91.92	91.92
86	91.92	95.96	98.99	98.99	98.99	98.99	97.98	98.99	98.99	98.99*
87	96.97	97.98	98.99	98.99	98.99	98.99	98.99	98.99	98.99	98.99*
88	97.98	97.98	98.99	98.99	98.99	98.99	98.99	98.99	98.99	98.99*
89	95.96	92.93	98.99	98.99	97.98	98.99	98.99	98.99	98.99	98.99
90	96.97	98.99	100.00	100.00	100.00	100.00	100.00	100.00	100.00	100.00*
91	48.48	48.48	48.48	48.48	48.48	48.48	48.48	48.48	48.48	48.48*
92	54.55	54.55	54.55	54.55	54.55	54.55	54.55	54.55	54.55	54.55*
93	32.32	32.32	32.32	32.32	32.32	32.32	32.32	32.32	32.32	32.32*
94	57.58	54.55	59.60	59.60	59.60	59.60	59.60	59.60	59.60	59.60*
95	73.74	76.77	81.82	81.82	81.82	81.82	81.82	81.82	81.82	81.82*
96	80.81	74.75	84.85	84.85	84.85	84.85	84.85	84.85	84.85	84.85*
97	86.87	91.92	94.95	94.95	94.95	94.95	94.95	94.95	94.95	94.95*
98	92.93	95.96	98.99	98.99	98.99	98.99	98.99	98.99	98.99	98.99*
99	66.67	63.64	63.64	64.65	67.68	67.68	67.68	67.68	62.63	67.68
100	74.75	77.78	81.82	81.82	81.82	81.82	81.82	81.82	81.82	81.82*

Table C.13: Coverage rate (in %) associated with the best integer solutions for each of the formulations. The grey background means that the instance has not been resolved.  $z^{Best}$  is the coverage rate (in %) of the best known integer solution for the considered instance and the presence of an asterisk means that it is the optimal solution. River instance group (4/4).

## Appendix D. Ranks

### Appendix D.1. Group 1: Peninsula

Instance	Base		Group 1						
	$R_{1,j}$	$R_{2,j}$	$R_{3,j}$	$R_{4,j}$	$R_{5,j}$	$R_{6,j}$	$R_{7,j}$	$R_{8,j}$	$R_{9,j}$
01	8.0	9.0	2.0	<b>1.0</b>	4.0	3.0	5.0	6.0	7.0
02	9.0	8.0	3.0	2.0	7.0	5.0	6.0	<b>1.0</b>	4.0
03	9.0	8.0	4.0	5.0	6.0	3.0	<b>1.0</b>	2.0	7.0
04	8.5	8.5	6.0	7.0	<b>1.0</b>	3.0	4.0	2.0	5.0
05	9.0	8.0	6.0	<b>1.0</b>	5.0	2.0	4.0	7.0	3.0
06	9.0	8.0	3.0	<b>1.0</b>	2.0	5.0	4.0	7.0	6.0
07	7.0	6.0	3.0	5.0	2.0	<b>1.0</b>	9.0	4.0	8.0
08	8.5	8.5	<b>1.0</b>	2.0	3.0	5.0	7.0	6.0	4.0
09	9.0	8.0	7.0	<b>1.0</b>	3.0	2.0	6.0	5.0	4.0
10	9.0	8.0	2.0	5.0	<b>1.0</b>	3.0	4.0	6.0	7.0
11	9.0	8.0	<b>1.0</b>	7.0	4.0	3.0	6.0	2.0	5.0
12	9.0	7.0	3.0	8.0	2.0	<b>1.0</b>	4.0	5.0	6.0
13	8.5	8.5	6.0	2.0	<b>1.0</b>	7.0	3.0	5.0	4.0
14	8.5	8.5	<b>1.0</b>	4.0	3.0	2.0	5.0	7.0	6.0
15	8.0	8.0	<b>1.0</b>	8.0	2.0	3.0	5.0	4.0	6.0
16	8.5	8.5	3.0	2.0	6.0	7.0	5.0	<b>1.0</b>	4.0
17	8.0	9.0	5.0	4.0	3.0	6.0	<b>1.0</b>	2.0	7.0
18	7.5	9.0	4.0	7.5	4.0	4.0	<b>1.0</b>	4.0	4.0
19	8.5	7.0	2.0	4.0	<b>1.0</b>	3.0	8.5	6.0	5.0
20	8.0	9.0	7.0	6.0	2.0	<b>1.0</b>	3.0	5.0	4.0
21	9.0	7.0	5.0	4.0	3.0	<b>1.0</b>	6.0	8.0	2.0
22	9.0	8.0	5.0	6.0	4.0	2.0	<b>1.0</b>	7.0	3.0
23	8.0	9.0	<b>1.0</b>	6.0	2.0	3.0	4.0	5.0	7.0
24	8.5	8.5	2.0	5.0	6.0	<b>1.0</b>	4.0	3.0	7.0
25	8.5	8.5	6.0	3.0	5.0	2.0	4.0	<b>1.0</b>	7.0
#Winner	0	0	5	4	4	5	4	3	0
$\sum_j R_{i,j}$	212.50	203.50	89.00	106.50	82.00	78.00	110.50	111.00	132.00
$\overline{R}_i$	8.50	8.14	3.56	4.26	3.28	3.12	4.42	4.44	5.28

Table D.14: Detail of the ranks for each of the formulations.  $R_{i,j}$  is the rank of model  $i \in \llbracket 1, 9 \rrbracket$  on instance  $j \in \llbracket 1, 25 \rrbracket$ . Peninsula instance group (1/4).



Appendix D.2. Group 2: Detroit

Instance	Base		Group 1						
	$R_{1,j}$	$R_{2,j}$	$R_{3,j}$	$R_{4,j}$	$R_{5,j}$	$R_{6,j}$	$R_{7,j}$	$R_{8,j}$	$R_{9,j}$
26	8.5	8.5	2.0	4.0	3.0	<b>1.0</b>	6.0	5.0	7.0
27	7.0	9.0	4.0	4.0	4.0	<b>1.0</b>	8.0	4.0	4.0
28	9.0	6.0	3.0	6.0	6.0	<b>1.5</b>	6.0	<b>1.5</b>	6.0
29	8.0	9.0	<b>1.0</b>	2.0	4.0	5.0	6.0	7.0	3.0
30	8.0	9.0	2.0	3.0	6.0	5.0	7.0	4.0	<b>1.0</b>
31	8.0	9.0	2.0	<b>1.0</b>	3.0	6.0	4.0	5.0	7.0
32	8.0	7.0	9.0	<b>1.0</b>	3.5	5.0	6.0	3.5	2.0
33	9.0	8.0	<b>1.0</b>	2.0	4.0	3.0	6.5	5.0	6.5
34	9.0	6.0	7.0	4.0	2.0	<b>1.0</b>	3.0	8.0	5.0
35	8.0	8.0	<b>2.5</b>	5.5	<b>2.5</b>	<b>2.5</b>	8.0	5.5	<b>2.5</b>
36	7.0	9.0	2.0	<b>1.0</b>	4.0	3.0	5.0	6.0	8.0
37	9.0	4.0	2.0	5.0	6.5	<b>1.0</b>	6.5	8.0	3.0
38	8.0	6.0	2.0	4.0	3.0	5.0	7.0	<b>1.0</b>	9.0
39	9.0	5.5	7.0	8.0	2.5	<b>1.0</b>	2.5	4.0	5.5
40	8.5	8.5	7.0	4.0	3.0	6.0	2.0	<b>1.0</b>	5.0
41	7.0	8.0	9.0	2.0	3.0	<b>1.0</b>	6.0	5.0	4.0
42	4.5	4.5	4.5	4.5	<b>1.0</b>	4.5	4.5	9.0	8.0
43	6.0	3.0	<b>1.0</b>	3.0	3.0	8.0	7.0	5.0	9.0
44	7.0	9.0	7.0	3.0	5.0	<b>1.0</b>	7.0	3.0	3.0
45	<b>2.0</b>	6.0	<b>2.0</b>	6.0	6.0	9.0	6.0	6.0	<b>2.0</b>
46	9.0	<b>2.0</b>	6.0	6.0	6.0	<b>2.0</b>	<b>2.0</b>	6.0	6.0
47	<b>1.0</b>	5.5	5.5	5.5	5.5	5.5	5.5	5.5	5.5
48	9.0	6.5	4.0	6.5	6.5	<b>2.0</b>	<b>2.0</b>	6.5	<b>2.0</b>
49	4.0	8.0	4.0	4.0	<b>1.5</b>	9.0	6.5	<b>1.5</b>	6.5
50	8.0	9.0	7.0	5.0	<b>2.5</b>	<b>2.5</b>	<b>2.5</b>	<b>2.5</b>	6.0
#Winner	2	1	5	3	4	12	3	5	4
$\sum_j R_{i,j}$	181.50	174.00	103.50	100.00	97.00	91.50	132.50	118.50	126.50
$\bar{R}_i$	7.26	6.96	4.13	4.00	3.88	3.66	5.30	4.74	5.05

Table D.15: Detail of the ranks for each of the formulations.  $R_{i,j}$  is the rank of model  $i \in \llbracket 1, 9 \rrbracket$  on instance  $j \in \llbracket 26, 50 \rrbracket$ . Detroit instance group (2/4).

Appendix D.3. Group 3: Island

Instance	Base		Group 1						
	$R_{1,j}$	$R_{2,j}$	$R_{3,j}$	$R_{4,j}$	$R_{5,j}$	$R_{6,j}$	$R_{7,j}$	$R_{8,j}$	$R_{9,j}$
51	8.0	9.0	5.0	2.0	6.0	4.0	7.0	3.0	<b>1.0</b>
52	8.0	9.0	<b>1.0</b>	5.0	2.0	3.0	6.0	4.0	7.0
53	9.0	8.0	5.0	6.0	3.0	4.0	2.0	<b>1.0</b>	7.0
54	8.5	8.5	2.0	<b>1.0</b>	6.0	3.0	5.0	4.0	7.0
55	7.5	6.0	4.5	7.5	2.5	<b>1.0</b>	4.5	2.5	9.0
56	9.0	6.5	<b>3.0</b>	<b>3.0</b>	6.5	<b>3.0</b>	<b>3.0</b>	<b>3.0</b>	8.0
57	8.0	9.0	<b>1.0</b>	7.0	6.0	5.0	2.0	4.0	3.0
58	8.0	8.0	2.5	8.0	2.5	<b>1.0</b>	5.0	4.0	6.0
59	8.0	9.0	5.5	<b>2.5</b>	5.5	<b>2.5</b>	7.0	<b>2.5</b>	<b>2.5</b>
60	7.0	8.0	6.0	<b>1.5</b>	4.0	4.0	9.0	<b>1.5</b>	4.0
61	9.0	8.0	5.5	<b>2.0</b>	<b>2.0</b>	5.5	<b>2.0</b>	5.5	5.5
62	9.0	8.0	4.5	4.5	4.5	<b>1.5</b>	<b>1.5</b>	4.5	7.0
63	7.0	7.0	2.0	7.0	7.0	3.0	7.0	<b>1.0</b>	4.0
64	9.0	7.0	<b>1.0</b>	5.0	3.5	2.0	3.5	7.0	7.0
65	8.0	9.0	5.0	3.5	7.0	2.0	6.0	3.5	<b>1.0</b>
66	7.5	5.0	6.0	9.0	3.0	3.0	3.0	7.5	<b>1.0</b>
67	9.0	4.0	4.0	<b>1.0</b>	4.0	4.0	4.0	7.5	7.5
68	8.5	8.5	4.0	2.0	5.0	<b>1.0</b>	6.0	3.0	7.0
69	9.0	8.0	<b>1.0</b>	4.0	5.0	3.0	6.0	7.0	2.0
70	8.5	8.5	6.0	4.0	<b>1.0</b>	7.0	5.0	3.0	2.0
71	9.0	5.0	4.0	3.0	6.0	<b>1.0</b>	2.0	7.0	8.0
72	8.5	8.5	5.0	4.0	<b>1.0</b>	3.0	2.0	7.0	6.0
73	8.5	8.5	3.0	6.0	4.0	7.0	5.0	2.0	<b>1.0</b>
74	9.0	8.0	7.0	2.0	5.0	<b>1.0</b>	3.0	4.0	6.0
75	9.0	8.0	6.0	7.0	2.0	<b>1.0</b>	4.0	3.0	5.0
#Winner	0	0	5	6	3	9	3	5	5
$\sum_j R_{i,j}$	209.50	192.00	99.50	107.50	104.00	75.50	110.50	102.00	124.50
$\bar{R}_i$	8.38	7.68	3.98	4.30	4.16	3.02	4.42	4.08	4.98

Table D.16: Detail of the ranks for each of the formulations.  $R_{i,j}$  is the rank of model  $i \in \llbracket 1, 9 \rrbracket$  on instance  $j \in \llbracket 51, 75 \rrbracket$ . Island instance group (3/4).

Appendix D.4. Group 4: River

Instance	Base		Group 1						
	$R_{1,j}$	$R_{2,j}$	$R_{3,j}$	$R_{4,j}$	$R_{5,j}$	$R_{6,j}$	$R_{7,j}$	$R_{8,j}$	$R_{9,j}$
76	8.0	9.0	7.0	3.0	4.0	<b>1.0</b>	2.0	5.0	6.0
77	8.0	9.0	6.0	2.0	4.0	<b>1.0</b>	3.0	5.0	7.0
78	8.0	9.0	5.0	4.0	6.0	2.0	3.0	7.0	<b>1.0</b>
79	8.5	8.5	2.0	<b>1.0</b>	6.0	5.0	7.0	4.0	3.0
80	9.0	8.0	2.0	<b>1.0</b>	5.0	4.0	6.0	3.0	7.0
81	8.0	9.0	<b>1.0</b>	2.0	3.0	4.0	7.0	5.0	6.0
82	8.5	8.5	<b>1.0</b>	3.0	4.0	5.0	6.0	7.0	2.0
83	9.0	8.0	5.0	3.0	<b>1.0</b>	4.0	7.0	6.0	2.0
84	9.0	8.0	5.0	2.0	4.0	<b>1.0</b>	7.0	6.0	3.0
85	8.0	9.0	5.0	6.0	2.0	3.0	7.0	4.0	<b>1.0</b>
86	9.0	8.0	4.0	2.0	6.0	<b>1.0</b>	7.0	5.0	3.0
87	9.0	8.0	4.0	6.0	<b>1.0</b>	3.0	2.0	7.0	5.0
88	8.5	8.5	7.0	4.0	2.0	3.0	<b>1.0</b>	6.0	5.0
89	8.0	9.0	<b>3.5</b>	<b>3.5</b>	7.0	<b>3.5</b>	<b>3.5</b>	<b>3.5</b>	<b>3.5</b>
90	9.0	8.0	7.0	5.0	3.0	<b>1.0</b>	6.0	4.0	2.0
91	8.0	9.0	2.0	<b>1.0</b>	3.0	4.0	6.0	5.0	7.0
92	8.0	9.0	3.0	<b>1.0</b>	2.0	5.0	7.0	4.0	6.0
93	9.0	8.0	5.0	2.0	7.0	4.0	6.0	3.0	<b>1.0</b>
94	8.0	9.0	7.0	4.0	5.0	6.0	2.0	3.0	<b>1.0</b>
95	9.0	8.0	2.0	3.0	7.0	6.0	4.0	<b>1.0</b>	5.0
96	8.0	9.0	<b>1.0</b>	2.0	4.0	6.0	7.0	3.0	5.0
97	9.0	8.0	3.0	5.0	7.0	<b>1.0</b>	6.0	2.0	4.0
98	9.0	8.0	7.0	6.0	3.0	2.0	4.0	<b>1.0</b>	5.0
99	8.0	9.0	6.0	4.0	3.0	2.0	5.0	<b>1.0</b>	7.0
100	9.0	8.0	6.0	7.0	4.0	3.0	2.0	<b>1.0</b>	5.0
#Winner	0	0	4	5	2	7	2	5	5
$\sum_j R_{i,j}$	212.50	212.50	106.50	82.50	103.00	80.50	123.50	101.50	102.50
$\bar{R}_i$	8.50	8.50	4.26	3.30	4.12	3.22	4.94	4.05	4.09

Table D.17: Detail of the ranks for each of the formulations.  $R_{i,j}$  is the rank of model  $i \in \llbracket 1, 9 \rrbracket$  on instance  $j \in \llbracket 76, 100 \rrbracket$ . River instance group (4/4).

## Appendix E. Two-way comparisons

### Appendix E.1. Group 1: Peninsula

$ M_i \succ M_j $	$M_1$	$M_2$	$M_3$	$M_4$	$M_5$	$M_6$	$M_7$	$M_8$	$M_9$	$\sum_j  M_i \succ M_j $
$M_1$	-	5	0	0	0	0	1	0	1	7
$M_2$	12	-	0	1	0	0	2	1	1	17
$M_3$	25	25	-	14	10	13	15	15	17	134
$M_4$	23	23	11	-	10	9	13	11	17	117
$M_5$	25	25	14	15	-	10	16	17	19	141
$M_6$	25	25	11	16	14	-	18	16	20	145
$M_7$	23	23	10	12	9	7	-	14	16	114
$M_8$	25	24	9	14	7	8	11	-	14	112
$M_9$	24	24	7	8	5	4	9	10	-	91
$\sum_i  M_i \succ M_j $	182	174	62	80	55	51	85	84	105	

Table E.18: Two-way comparisons for all formulations where  $M_i \succ M_j$  means that the formulation  $M_i$  (strictly) dominates the formulation  $M_j \forall i, j \in \llbracket 1, 9 \rrbracket$  with  $i \neq j$ .  $\sum_j |M_i \succ M_j|$  accounts for the number of times that model  $j$  is strictly dominated and  $\sum_i |M_i \succ M_j|$  accounts for the number of times that model  $i$  strictly dominates. Peninsula instance group (1/4).

### Appendix E.2. Group 2: Detroit

$ M_i \succ M_j $	$M_1$	$M_2$	$M_3$	$M_4$	$M_5$	$M_6$	$M_7$	$M_8$	$M_9$	$\sum_j  M_i \succ M_j $
$M_1$	-	11	3	2	2	4	5	3	6	36
$M_2$	10	-	5	3	2	3	3	5	4	35
$M_3$	18	18	-	12	12	9	14	13	11	107
$M_4$	21	16	8	-	9	11	15	12	14	106
$M_5$	23	18	9	9	-	9	16	12	13	109
$M_6$	20	19	13	12	13	-	15	14	16	122
$M_7$	17	16	8	6	3	5	-	9	11	75
$M_8$	22	17	9	6	5	8	13	-	11	91
$M_9$	18	18	9	6	7	6	9	10	-	83
$\sum_i  M_i \succ M_j $	149	133	64	56	53	55	90	78	86	

Table E.19: Two-way comparisons for all formulations where  $M_i \succ M_j$  means that the formulation  $M_i$  (strictly) dominates the formulation  $M_j \forall i, j \in \llbracket 1, 9 \rrbracket$  with  $i \neq j$ .  $\sum_j |M_i \succ M_j|$  accounts for the number of times that model  $j$  is strictly dominated and  $\sum_i |M_i \succ M_j|$  accounts for the number of times that model  $i$  strictly dominates. Detroit instance group (2/4).

Appendix E.3. Group 3: Island

$ M_i \succ M_j $	$M_1$	$M_2$	$M_3$	$M_4$	$M_5$	$M_6$	$M_7$	$M_8$	$M_9$	$\sum_j  M_i \succ M_j $
$M_1$	-	6	0	1	0	0	1	0	1	9
$M_2$	12	-	1	2	1	0	1	3	4	24
$M_3$	25	23	-	11	12	8	13	10	15	117
$M_4$	21	21	12	-	11	7	11	10	14	107
$M_5$	24	21	9	11	-	6	12	11	16	110
$M_6$	25	24	14	16	16	-	15	15	15	140
$M_7$	23	22	9	11	8	6	-	10	16	105
$M_8$	24	21	12	10	12	7	14	-	13	113
$M_9$	24	20	9	10	8	7	9	8	-	95
$\sum_i  M_i \succ M_j $	178	158	66	72	68	41	76	67	94	

Table E.20: Two-way comparisons for all formulations where  $M_i \succ M_j$  means that the formulation  $M_i$  (strictly) dominates the formulation  $M_j \forall i, j \in \llbracket 1, 9 \rrbracket$  with  $i \neq j$ .  $\sum_j |M_i \succ M_j|$  accounts for the number of times that model  $j$  is strictly dominated and  $\sum_i |M_i \succ M_j|$  accounts for the number of times that model  $i$  strictly dominates. Island instance group (3/4).

Appendix E.4. Group 4: River

$ M_i \succ M_j $	$M_1$	$M_2$	$M_3$	$M_4$	$M_5$	$M_6$	$M_7$	$M_8$	$M_9$	$\sum_j  M_i \succ M_j $
$M_1$	-	11	0	0	0	0	0	0	0	11
$M_2$	11	-	0	0	0	0	0	0	0	11
$M_3$	25	25	-	8	12	8	14	12	12	116
$M_4$	25	25	16	-	17	11	17	16	13	140
$M_5$	25	25	13	8	-	10	15	13	13	122
$M_6$	25	25	16	13	15	-	19	14	15	142
$M_7$	25	25	10	7	10	5	-	7	10	99
$M_8$	25	25	12	8	12	10	17	-	12	121
$M_9$	25	25	12	11	12	9	14	12	-	120
$\sum_i  M_i \succ M_j $	186	186	79	55	78	53	96	74	75	

Table E.21: Two-way comparisons for all formulations where  $M_i \succ M_j$  means that the formulation  $M_i$  (strictly) dominates the formulation  $M_j \forall i, j \in \llbracket 1, 9 \rrbracket$  with  $i \neq j$ .  $\sum_j |M_i \succ M_j|$  accounts for the number of times that model  $j$  is strictly dominated and  $\sum_i |M_i \succ M_j|$  accounts for the number of times that model  $i$  strictly dominates. River instance group (4/4).

Appendix E.5. Synthesis

$ M_i \succ M_j $	$M_1$	$M_2$	$M_3$	$M_4$	$M_5$	$M_6$	$M_7$	$M_8$	$M_9$	$\sum_j  M_i \succ M_j $
$M_1$	-	33	3	3	2	4	7	3	8	63
$M_2$	45	-	6	6	3	3	6	9	9	87
$M_3$	93	91	-	45	46	38	56	50	55	474
$M_4$	90	85	47	-	47	38	56	49	58	470
$M_5$	97	89	45	43	-	35	59	53	61	482
$M_6$	95	93	54	57	58	-	67	59	66	549
$M_7$	88	86	37	36	30	23	-	40	53	393
$M_8$	96	87	42	38	36	33	55	-	50	437
$M_9$	91	87	37	35	32	26	41	40	-	389
$\sum_i  M_i \succ M_j $	695	651	271	263	254	200	347	303	360	

Table E.22: Two-way comparisons for all formulations where  $M_i \succ M_j$  means that the formulation  $M_i$  (strictly) dominates the formulation  $M_j \forall i, j \in \llbracket 1, 9 \rrbracket$  with  $i \neq j$ .  $\sum_i |M_i \succ M_j|$  accounts for the number of times that model  $j$  is strictly dominated and  $\sum_j |M_i \succ M_j|$  accounts for the number of times that model  $i$  strictly dominates. All instances.

## Appendix F. Instances

### Appendix F.1. Group 1: Peninsula

Grid	Instance	$n_{TxRx}$		$n_{Tx}$		$n_{Rx}$			
		$A_{HF}$	$B_{LF}$	$C_{HF}$	$D_{LF}$	$E_{HF}$	$F_{HF}$	$G_{LF}$	$H_{LF}$
<p>Data from GEBCO (raw DEM) Down-sampling procedure</p> <p>9.82 km (<math>\approx 1091.48</math> m / cell)</p> <p>12.51 km (<math>\approx 1389.94</math> m / cell)</p> <p>9 x 9 (81 cells)</p> <p>70 maritime &amp; 11 terrestrial</p>	01	-	-	1	-	1	1	-	-
	02	-	-	1	-	2	1	-	-
	03	-	-	1	-	2	2	-	-
	04	-	-	2	-	2	2	-	-
	05	-	-	1	1	2	1	1	-
	06	-	-	1	1	2	1	1	1
	07	1	-	-	1	2	-	1	-
	08	1	-	1	-	2	1	-	-
	09	2	-	1	-	2	2	-	-
	10	1	1	-	-	1	1	-	-
	11	-	-	1	1	1	1	1	1
	12	1	1	-	-	2	2	-	-
	13	1	-	2	-	3	3	-	-
	14	1	-	-	1	2	2	1	-
	15	-	1	2	-	4	4	-	-
	16	-	-	2	-	2	4	-	-
	17	-	-	1	1	2	2	2	1
	18	1	-	1	1	2	2	1	-
	19	1	-	2	-	2	4	-	-
	20	-	-	3	-	3	3	-	-
	21	1	-	-	1	-	-	1	1
	22	1	-	-	1	-	-	1	2
	23	1	-	-	1	-	-	2	2
	24	-	1	-	1	-	-	1	2
	25	-	1	-	1	-	-	1	1

Table F.23: *Tour d'horizon* of the instance library: peninsula group (1/4).

Appendix F.2. Group 2: Detroit

Grid	Instance	$n_{T \times R_x}$		$n_{T_x}$		$n_{R_x}$			
		$A_{HF}$	$B_{LF}$	$C_{HF}$	$D_{LF}$	$E_{HF}$	$F_{HF}$	$G_{LF}$	$H_{LF}$
	26	1	1	1	-	2	2	-	-
	27	1	-	-	1	2	1	1	-
	28	1	-	-	1	2	1	1	1
	29	-	-	1	-	1	1	-	-
	30	-	-	1	-	2	1	-	-
	31	-	-	1	-	2	2	-	-
	32	1	-	1	-	2	2	-	-
	33	1	-	1	-	3	2	-	-
	34	1	-	1	-	3	3	-	-
	35	1	-	2	-	3	3	-	-
Data from GEBCO (raw DEM) Down-sampling procedure	36	1	-	-	-	2	2	-	-
	37	1	-	-	1	1	1	1	-
	38	1	-	-	1	2	1	1	2
	39	-	-	1	1	2	1	1	1
	40	-	-	1	1	2	1	2	1
	41	-	-	1	1	2	2	2	2
	42	-	-	2	1	1	1	-	1
	43	-	-	2	1	2	1	-	1
	44	-	-	2	1	2	2	-	1
	45	2	-	-	1	1	-	-	1
	46	2	-	-	1	1	1	-	1
12 x 12 (144 cells) 81 maritime & 63 terrestrial	47	1	-	-	2	1	-	1	-
48	1	-	-	1	1	1	1	1	
49	-	-	3	1	2	1	-	1	
50	-	-	3	1	1	1	-	1	

Table F.24: *Tour d'horizon* of the instance library: detroit group (2/4).



Appendix F.3. Group 3: Island

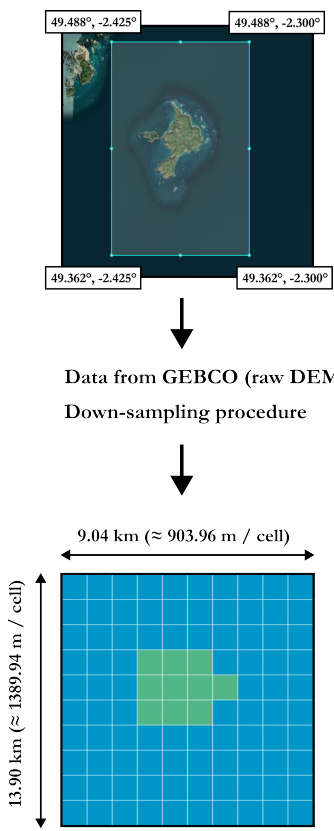
Grid	Instance	$n_{T \times R_x}$		$n_{T_x}$		$n_{R_x}$			
		$A_{HF}$	$B_{LF}$	$C_{HF}$	$D_{LF}$	$E_{HF}$	$F_{HF}$	$G_{LF}$	$H_{LF}$
 <p>Data from GEBCO (raw DEM) Down-sampling procedure</p> <p>9.04 km (<math>\approx 903.96</math> m / cell)</p> <p>13.90 km (<math>\approx 1389.94</math> m / cell)</p> <p>10 x 10 (100 cells)</p> <p>90 maritime &amp; 10 terrestrial</p>	51	-	-	1	-	1	1	-	-
	52	-	-	1	-	1	2	-	-
	53	-	-	1	-	2	2	-	-
	54	-	-	2	-	2	2	-	-
	55	1	-	2	-	2	2	-	-
	56	2	-	2	-	2	2	-	-
	57	2	-	2	-	3	3	-	-
	58	1	-	2	-	2	4	-	-
	59	1	-	2	-	3	3	-	-
	60	1	-	2	-	4	4	-	-
	61	2	-	1	-	1	2	-	-
	62	2	-	1	-	2	3	-	-
	63	2	-	1	-	4	4	-	-
	64	-	-	1	1	1	1	1	1
	65	-	-	1	1	2	1	2	1
	66	-	-	1	1	2	2	2	2
	67	-	-	2	1	3	3	2	2
	68	1	-	1	-	1	-	-	-
	69	-	1	-	1	-	-	1	-
	70	-	1	-	1	-	-	1	1
	71	1	-	-	1	1	1	1	-
	72	-	1	-	1	-	-	2	1
	73	-	1	-	1	-	-	-	2
	74	1	1	-	-	2	-	1	-
	75	1	1	-	-	2	-	2	-

Table F.25: *Tour d'horizon* of the instance library: island group (3/4).

Appendix F.4. Group 4: River

Grid	Instance	$n_{T \times R \times}$		$n_{T \times}$		$n_{R \times}$			
		$A_{HF}$	$B_{LF}$	$C_{HF}$	$D_{LF}$	$E_{HF}$	$F_{HF}$	$G_{LF}$	$H_{LF}$
	76	-	-	1	-	1	1	-	-
	77	-	-	1	-	2	1	-	-
	78	-	-	2	-	2	2	-	-
	79	1	-	2	-	2	2	-	-
	80	1	-	1	-	2	2	-	-
	81	1	-	1	-	3	3	-	-
	82	2	-	1	-	3	3	-	-
	83	2	1	1	-	3	3	-	-
	84	2	1	1	-	2	1	2	1
	85	2	1	1	-	2	2	2	1
Data from GEBCO (raw DEM) Down-sampling procedure	86	2	1	1	1	2	2	2	2
	87	3	1	-	1	2	2	2	2
	88	2	2	-	1	2	-	-	2
	89	-	-	3	3	2	4	4	2
	90	-	-	3	3	4	4	4	4
	91	1	-	-	1	-	-	1	-
	92	1	-	-	1	-	-	1	1
	93	-	-	-	1	-	-	1	1
	94	1	-	-	1	2	1	1	1
	95	-	1	1	1	1	1	2	2
	96	-	1	1	1	1	1	3	3
	97	-	1	1	2	1	1	3	3
	98	-	2	1	2	1	1	3	3
99 maritime & 385 terrestrial	99	-	-	2	2	2	-	2	-
	100	-	-	-	3	-	-	3	3

Table F.26: *Tour d'horizon* of the instance library: river group (4/4).